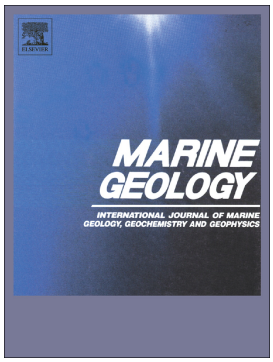

Iron, copper, and zinc isotopic fractionation in seafloor basalts and hydrothermal sulfides

Zhigang Zeng, Xiaohui Li, Shuai Chen, Jeroen de Jong, Nadine Mattielli, Haiyan Qi, Christopher Pearce, Bramley J. Murton

PII: S0025-3227(21)00073-6

DOI: https://doi.org/10.1016/j.margeo.2021.106491

Reference: MARGO 106491

To appear in: *Marine Geology*

Received date: 25 July 2020

Revised date: 9 April 2021

Accepted date: 13 April 2021

Please cite this article as: Z. Zeng, X. Li, S. Chen, et al., Iron, copper, and zinc isotopic fractionation in seafloor basalts and hydrothermal sulfides, *Marine Geology* (2021), https://doi.org/10.1016/j.margeo.2021.106491

Iron, copper, and zinc isotopic fractionation in seafloor basalts and hydrothermal sulfides

Zhigang Zeng[a,b,c,d,*], Xiaohui Li[a,d], Shuai Chen[a], Jeroen de Jong[e], Nadine Mattielli[e], Haiyan Qi[a,d], Christopher Pearce[f], Bramley J. Murton[f]

[a] Seafloor Hydrothermal Activity Laboratory, CAS Key Laboratory of Marine Geology and Environment, Institute of Oceanology, Chinese Academy of Sciences, Qingdao 266071, China

[b] Laboratory for Marine Mineral Resources, Qingdao National Laboratory for Marine Science and Technology, Qingdao 266071, China

[c] University of Chinese Academy of Sciences, Beijing 100049, China

[d] Center for Ocean Mega-Science, Chinese Academy of Sciences, 7 Nanhai Road, Qingdao, 266071, China

[e] Laboratoire G-Time, Département des Géosciences, Environnement et Société, Université Libre de Bruxelles, CP 160/02, 1050 Brussels, Belgium

[f] National Oceanography Centre, European Way, Southampton SO14 3ZH, UK

*Corresponding author. Email address: zgzeng@ms.qdio.ac.cn (Z.-G. Zeng).

Abstract

Studies of the Fe, Cu, and Zn isotopic compositions of volcanic rocks and sulfides provide an important tool for understanding magmatic, hydrothermal, and alteration processes, thereby enabling the determination of both transition metal sources and the

quantification of the petrologic environmental impacts of hydrothermal activities. In this study, the $\delta^{56}Fe$ and $\delta^{57}Fe$ values of the mid-ocean ridge basalts (MORBs) are higher than those of the seafloor hydrothermal fluids, while the reverse is true for the $\delta^{66}Zn$ and $\delta^{68}Zn$ values, suggesting that basalt-fluid interactions preferentially incorporate isotopically light Fe and heavy Zn into the fluids, resulting in the relative enrichment of heavier Fe and lighter Zn isotopes in altered basaltic rocks. Most of the $\delta^{56}Fe$ values (−1.96 to +0.11‰) of the sulfide minerals are within the range of the vent fluids, but they are significantly lower than those of the MORBs and back-arc basin basalts (BABBs), suggesting that the Fe in the sulfides was mainly derived from the fluids. However, the majority of the chalcopyrite $\delta^{56}Fe$ and $\delta^{57}Fe$ values are higher than those of the sphalerite and pyrite. This suggests that high-temperature sulfide minerals are enriched in ^{56}Fe and ^{57}Fe, whereas medium- and low-temperature sulfides are depleted in ^{56}Fe and ^{57}Fe. Moreover, the $\delta^{65}Cu$ (−0.88 to −0.16‰) and $\delta^{66}Zn$ (−0.39 to −0.03‰) values of the sulfide minerals are significantly lower than those of the MORBs, BABBs, and fluids, suggesting that ^{63}Cu and ^{64}Zn were preferentially removed from the fluids and incorporated into the chalcopyrite and sphalerite, respectively. Consequently, vent fluid injection and deposition can cause the heavier Cu and Zn isotopic compositions of hydrothermal plumes, seawater, and sediments.

Keywords: Fe-Cu-Zn isotopic fractionation; mid-ocean ridge basalts; seafloor hydrothermal sulfides; magmatic processes and ore formation

1. Introduction

Seafloor hydrothermal fields often contain polymetallic massive sulfides, chimneys, mounds, and their host rocks (e.g., basalts). Both high (>300°C) and low temperature (<300°C) assemblages consisting of varying proportions of pyrite, chalcopyrite, and sphalerite have been found to be common in the most massive sulfides, chimneys, and mounds in mid-ocean ridge and back-arc basin settings (e.g., Hannington et al., 1991; Herzig and Hannington, 1995; Fouquet et al., 2018). Chalcopyrite has also been found in the host mafic rocks; however, pyrite and sphalerite are unlikely to be a primary minerals in basalts (Francis, 1990) and are usually common hydrothermal and sedimentary minerals. Copper (Cu) can be in dispersed in sulfides in mid-ocean ridge basalts (MORBs) (Doe, 1994). For example, rounded to sub-rounded globules of sulfide minerals (chalcopyrite and Ni-bearing pyrrhotite) occur as inclusions in glass or in phenocrysts in seafloor basalts from the Siqueiros Fracture Zone, Indian Ocean, and Lau Basin (Francis, 1990). Zinc (Zn) is a mildly incompatible element and is enriched in the glass phase relative to olivine because Zn does not fit into the structure of plagioclase. The average Zn and Cu contents of seafloor MORBs are 75 and 75 ppm (Doe, 1994), respectively; and Fe^{2+}, which is a major element in MORBs, substitutes readily for Mg in all of the relevant crystallizing phases (O´Neill et al., 2018).

The stable isotopic systematics of iron (Fe), copper, and zinc have been applied extensively as a tool for tracking fluid pathways and for fingerprinting sources of volcanic rocks and seafloor hydrothermal systems (e.g., Zhu et al., 2000; Sharma et al., 2001; Rouxel et al., 2004a, 2004b; John et al., 2008; Liu et al., 2015). The Fe isotopic systematics of MORBs, ocean island basalts (OIBs), and back-arc basin basalts (BABBs) have demonstrated that MORBs and BABBs have homogeneous Fe isotopic compositions, while OIBs are isotopically heterogeneous (Weyer & Ionov, 2007; Schuessler et al., 2009; Teng et al., 2013; Williams and Bizimis, 2014). However, in the olivine phenocrysts in Hawaiian OIBs, evidence of significant Fe isotopic fractionation during magmatic differentiation has been observed on both the whole-rock and crystal scales (Teng et al., 2008, 2011). The Fe isotopic compositions of the silicate minerals in peridotite and pyroxenite xenoliths in Hawaiian OIBs were also analyzed to explore the use of Fe isotopes as a tracer of both peridotite and pyroxenite components in the source of OIBs (Williams and Bizimis, 2014). Moreover, the Fe isotopic compositions of the altered oceanic basalts from ODP Site 801C in the Mariana Trench exhibit depleted light Fe isotopes relative to those of fresh basalts, suggesting the preferential leaching of light Fe during alteration of Mariana arc basalts (Rouxel et al., 2003).

Various volcanic rock types, including MORBs, OIBs, island arc basalts, and subduction-related andesites and dacites, have been systematically analyzed to investigate Cu isotopic fractionation during mantle metasomatism and partial melting and to

characterize the Cu isotopic compositions of the distinct silicate reservoirs in the Earth (Ben Othman et al., 2006; Herzog et al., 2009; Li et al., 2009; Liu et al., 2015). However, the Cu and Zn isotopic compositions of altered oceanic crust recovered from IODP Site 1256 on the East Pacific Rise (EPR) indicate that low-temperature hydrothermal alteration results in limited Cu and Zn isotopic fractionation in altered oceanic crust, while significant Cu and Zn isotopic fractionation occurs during high-temperature hydrothermal alteration of mid-ocean ridge rocks (Vance et al., 2008; Little et al., 2014; Huang et al., 2016). Moreover, high-precision Zn isotope data for MORBs and OIBs have revealed that MORBs exhibit homogeneous δ^{66}Zn values (+0.25‰ to +0.30‰; Ben Othman et al., 2006; Doucet et al., 2016; Wang et al., 2017), which are similar to those of OIBs (+0.31±0.09‰; Herzog et al., 2009; Chen et al., 2013; Wang et al., 2017). Ben Othman et al. (2006) also reported that MORBs from different ocean basins exhibit little variation from their average composition of δ^{66}Zn = +0.25‰. Moreover, it has been established that the δ^{66}Zn values of four andesitic samples from the Merapi island arc volcano are homogeneous, with values between +0.23‰ and +0.25‰ (Toutain et al., 2008).

Thus far, the Fe isotopic compositions of seafloor hydrothermal sulfides have been determined for hydrothermal systems on mid-ocean ridges (Sharma et al., 2001; Severmann et al., 2004; Rouxel et al., 2004a, 2008; German et al., 2008; Bennett et al., 2009). On the Juan de Fuca Ridge, the hydrothermal fluids venting into the overlying

water column provide a source of light Fe isotopes to the deep oceans and contribute to the Fe isotope variations observed in seafloor sediments from the mid-ocean ridge in the northeast Pacific (Sharma et al., 2001; Chu et al., 2006). The Fe isotopic composition of the plume particles in the Rainbow hydrothermal field on the Azorean segment of the Mid-Atlantic Ridge (MAR) has remained invariant over at least the past 16,000 years, implying that changing the Fe isotopic composition of the seawater in the North Atlantic Ocean requires changes in the relative fluxes of Fe to the ocean (Beard et al., 2003a; Severmann et al., 2004). However, in the Lucky Strike hydrothermal field of the MAR, the light Fe isotopic compositions (as low as 3.2‰) can be explained by equilibrium fractionation during sulfide precipitation in a subsurface environment, which provides further evidence for abiotic fractionation of Fe isotopes in hydrothermal systems in the North Atlantic Ocean (Rouxel et al., 2004a). A study of the δ^{56}Fe values of the 5°S hydrothermal fields on the MAR concluded that a stable, dissolved Fe fraction may have an isotopic signature that is heavier than that of the original hydrothermal fluid, and this fraction could be used to trace hydrothermally sourced dissolved Fe throughout the deep-ocean (Bennett et al., 2009). Furthermore, in the hydrothermal fields on the EPR between 9°N and 10°N, the δ^{56}Fe values of the marcasite/pyrite of a single chimney are lower than those of the chalcopyrite and fluids, suggesting that the Fe isotopes of the sulfides and fluids are in disequilibrium, which can be explained by isotopic exchange during the precipitation of pyrite or during the rapid formation of pyrite from FeS in

mid-ocean ridges (Sharma et al., 2001; Rouxel et al., 2008; Polyakov and Soultanov, 2010).

The Cu isotopic compositions of MAR sulfides indicate that the subsurface precipitation of Cu-rich sulfides does not significantly control the δ^{65}Cu values of the hydrothermal chimneys, and the oxidation of primary Cu-sulfides may be the major cause of Cu isotopic fractionation in hydrothermal systems (up to 3‰) (Shields et al., 1965; Rouxel et al., 2004b; Markl et al., 2006; Fernandez and Borrok, 2009). However, the presence of mid-ocean ridge sulfides (MORSs) with heavy δ^{65}Cu values can be explained by the processes occurring on the seafloor, such as the hydrothermal reworking of previously altered sulfides by high-temperature fluids, while sulfides with negative δ^{65}Cu values may have undergone extensive recrystallization (Rouxel et al., 2004b; Mason et al., 2005). Furthermore, the chalcopyrite from the sulfide chimneys at 21°N and 13°N on the EPR, at 86°W in the Galapagos Rift in the Pacific, and in the Broken Spur field at 29°N on the MAR, exhibit a larger variation in δ^{65}Cu values, from −4.81 to +11.47‰ (Zhu et al., 2000). The δ^{65}Cu variations of these MORSs can be explained using a two-stage model, which involves the preferential leaching of δ^{65}Cu during hydrothermal processes and the subsequent isotopic exchange between the crystallized Cu-sulfides and fluids (Zhu et al., 2000; Mason et al., 2005; Markl et al., 2006). The variation in the δ^{65}Cu values of the seafloor hydrothermal vents in back-arc basins (eastern Manus basin, North Fiji back-arc basin (NFB), and northeastern Lau basin) and island arc settings (Tonga Arc) in the

western Pacific (Kim et al., 2014) may be attributed to Cu isotope fractionation during the alteration and redox reactions associated with the maturation of venting sites near the surface (Rouxel et al., 2004b; Pękala et al., 2011; Kim et al., 2014).

The Zn isotopic compositions of the vent fluids of mid-ocean ridges and those of chimney sulfides indicate that there are large variations in the δ^{66}Zn values of hydrothermal fluids, which has been interpreted to suggest that Zn sulfide precipitation is a primary factor causing the variations in the δ^{66}Zn values of fluids (Mason et al., 2005; John et al., 2008; Fernandez and Borrok, 2009). However, the Cu and Zn isotopic compositions of the hydrothermal fluids of the eastern Manus back-arc basin indicate the systematic enrichment of heavy Cu (δ^{65}Cu = +0.3 ± 0.2‰) and Zn (δ^{66}Zn = –0.04 to +0.94‰) isotopes, which has been interpreted to be the result of subseafloor precipitation/redissolution processes, rather than the result of the evaporation/condensation of metal-rich magmatic fluids at a certain depth (Dekov and Rouxel, 2012).

In this study, Fe, Cu, and Zn isotopic analyses were performed on MORS, back-arc basin sulfides (BABS), and their host MORBs collected from the EPR near 13°N, the EPR between 1° and 2°S, the Edmond hydrothermal field (EHF) on the Central Indian Ridge (CIR), A area on the Southwest Indian Ridge (SWIR), and the Sonne 99 hydrothermal field (S99HF) in the NFB (Fig. 1). Our findings may aid in 1) revealing the Fe-Cu-Zn isotopic characteristics of the MORBs, MORS, and BABS, 2) determining the sources of

these metals, and 3) investigating the effects of the fluid-rock interactions and mixing between the fluids and seawater on the Fe-Cu-Zn isotopic compositions of the MORS and BABS, which will improve our understanding of the relationships between the sulfides and their host volcanic rocks as well as the hydrothermal processes involved in the transfer of Fe, Cu, and Zn between mantle sources, hydrothermal fluids, host rocks, and sulfides.

2. Sampling and methods

2.1. Sample Collection, Descriptions, and Processing

The studied MORS and BABS, which formed from both focused high-temperature (>300°C) fluid outflow through chimneys and from medium- (300 to 200 °C) to low-temperature (<200°C) fluids expelled from mounds (Michard et al., 1984; Merlivat et al., 1987; Bowers et al., 1988; Ishibashi et al., 1994a, 1994b; Koschinsky et al., 2002; Gallant and Von Damm, 2006; Schmidt et al., 2007), as well as their host MORBs and BABBs, respectively (e.g., Kumagai et al., 2008; Zeng et al., 2010, 2014, 2015a, 2015b), were recovered from seafloor hydrothermal fields using a TV-grab sampler in 2005, 2007, 2008, 2009, and 2010 during the DY105-17, DY115-19, DY115-20, and DY115-21 cruises of the R/V Dayang Yihao, respectively (Zeng et al., 2014, 2015a, 2015b, 2017). The BABS samples from the S99HF in the NFB were collected in 1998, during the

SO134 cruise of the R/V Sonne for the German HYFIFLUX II project. In the NFB, the S99HF is located directly south of the triple junction point at 16°50′S, and it is hosted by basaltic rocks, the trace element compositions of which indicate that the magma generation was influenced by two different sources: normal MORB and OIB related to enriched MORB (Eissen et al., 1994; Nohara et al., 1994; Koschinsky et al., 2002; Kim et al., 2006).

Tables S1 and S2 and Figure 1 present information regarding the sampling locations and depths and the mineral compositions of the MORS, BABS, and their host MORBs. The major minerals of the host MORBs included olivine and plagioclase, with minor clinopyroxene and orthopyroxene. The MORS and BABS mineral aggregate samples consisted of major pyrite ± marcasite, chalcopyrite, sphalerite, anhydrite, barite, opal, minor galena, and amorphous silica (Table S2). The descriptions of the sulfide samples and related mineralogy were detailed by Zeng et al. (2014). The sulfide minerals from the EPR 13°N and the Edmond field used for the isotopic analysis include pyrite, chalcopyrite, and sphalerite. Pyrite and chalcopyrite were used for EPR1−2°S; whereas for EPR13°N, and A area in the SWIR, only pyrite was concentrated for this study.

The fresh MORB chips were powdered (200 mesh) using an agate mortar for the Fe, Cu, and Zn isotopic analyses. All of the MORS and BABS samples were crushed using a jaw crusher and then sieved to obtain coarse grains (~5 mm in size). First, the coarse grains were examined with the naked eye to exclude grains with apparent oxidation. Then, they

were crushed using an agate mortar and pestle and were sieved to obtain sulfide mineral grains between 50 μm and 2 mm in size, which were subsequently treated (e.g., ethanol elutriation) (Zeng et al., 2014, 2015a, 2015b, 2017). As most of the samples were fine grained and contained intergrown phenocrysts, an integrated mechanical separation method (involving a high-frequency dielectric splitter, a magnetic separator, and an electromagnetic separator) was used to obtain a monomineralic sulfide as described in Zeng et al. (2017). Thereafter, the sulfide minerals were carefully manually selected under a binocular microscope to avoid sulfates and oxides, and then, they were ultrasonically cleaned in ultrapure alcohol to remove any seawater influences (Zeng et al., 2014). Finally, all the sulfide mineral samples were ground to a <63 μm powder using an agate mortar for major and trace elements, Fe, Cu, and Zn isotopic analyses.

2.2. Major and trace element analyses

The major and trace element compositions of the volcanic rocks were determined using an X-ray fluorescence spectrometer (XRF) and an inductively coupled plasma-mass spectrometer (ICP-MS, ELAN DRC II), respectively, at the China National Nuclear Corporation (CNNC), Beijing Research Institute of Uranium Geology. First, 0.9 g of sample powder was mixed with 9.0 g $Li_2B_4O_7$ to produce specially made glass disks at 1050−1100°C in an automatic melting instrument. Loss on ignition (LOI) values were determined from the weight difference after ignition at 1000°C. The accuracy of the

analytical procedure was assessed using certified reference materials (GBW07112) (Table S3). The precision of the analysis was better than ±5%. The accuracy was better than 5% for SiO_2, Al_2O_3, Fe_2O_3, MgO, CaO, Na_2O, and K_2O; and it was better than 9% for TiO_2, MnO, and P_2O_5.

Forty milligrams of whole-rock powder were dissolved in a Teflon beaker using a mixture of 0.5 mL of concentrated HNO_3 and 1.5 mL of HF, which was heated at 150°C for 24 h. Then, 0.2 mL of $HClO_4$ was added and the temperature was maintained at 120°C. When no more $HClO_4$ volatilized from the Teflon beaker, 1 mL of HNO_3 and 1 mL of Milli-Q water (18.2 MΩ•cm) were added to redissolve the residue. After this, the solution was cooled and diluted 1000 times with pure 2% HNO_3, and then, the solution was analyzed for trace elements. The analytical results of the reference materials (GBW07104 and GBW07312) agree well with the certified values (Table S4). The ICP-MS detection limits of the rare earth elements (REEs) and other trace elements were 0.001–0.1 μg/g; and the analytical accuracy of each measured element was better than 5%.

2.3. Fe, Cu, and Zn Isotopic Analyses

The isotopic ratios of all of the MORB, MORS, and BABS samples were measured on either the Nu Plasma I (Zn in basalts) or the Nu Plasma II (Fe, Cu, and Zn in basalts and sulfides) multiple collector-inductively coupled plasma-mass spectrometer (MC-ICP-MS,

Nu Instruments, Wrexham, UK) at the Université Libre de Bruxelles (ULB, Laboratoire G-Time), Brussels, Belgium. The dissolution; the Fe, Cu, and Zn purifications; and the isotopic analyses were conducted using the established procedure described by Petit et al. (2008) and Sossi et al. (2015), which was slightly modified, following the method of Debret et al. (2018). In brief, the powdered samples (approximately 5 mg for the sulfide minerals and 50 mg for the bulk rocks) were dissolved in closed screw-top Savillex Teflon beakers using a mixture of double-distilled concentrated HF, HNO_3, and HCl for a minimum of ~3 days at 125°C. After complete dissolution was achieved, 1 ml of 8 N HCl + 0.001% H_2O_2 was added to the beaker, and the solution was heated to dryness at 80°C. This process was repeated two or three times to ensure that all the cations were converted into chloride species. The final residues were dissolved in 1 ml of 8 N HCl + 0.001% H_2O_2 in preparation for the ion exchange separation. The Fe, Cu, and Zn in the samples were separated from the sample matrix constituents (e.g., Ti, Cr, and Mg) using an anion exchange resin (Bio-Rad AG1-X8, 100 to 200 mesh) in an HCl medium. A second passage for the Cu and Zn was preferred to avoid any spectral or non-spectral interferences from the potential residual matrix elements during the isotopic analysis. The Cu and Zn isotope ratios were measured using the doping method with the addition of a JMC Zn (Art. Nr 13835, lot Nr 0620611.10, ‘Zn110’) or Cu (Art. Nr 13867, lot Nr 13.0140203.10, ‘Cu310’) in-house standard solution, and the sample-standard bracketing technique (Petit et al., 2008). The isotopic determinations of the Zn in the basalts were

carried out in the wet plasma mode, while the Cu in the basalts and sulfides and the Zn in the sulfides were analyzed under higher sensitivity dry plasma conditions using an ESL Apex-Q desolvator (Elemental Scientific, Omaha, Nebraska, USA). The solution concentrations for the measurements were 400 μg/L of Zn (wet plasma) and 100 μg/L of Zn or Cu (dry plasma) in 0.05 M HNO_3.

To monitor the accuracy of the analyses and to report the data, the SRM NIST 976 Cu and Lyon JMC 3-0749L Zn reference solutions and the IRMM 3702 Zn certified reference material were measured (Ponzevera et al., 2006). The Cu and Zn isotopic data are reported in standard δ notation in per-mil (‰) against international reference materials SRM NIST 976 and JMC 3-0749L, respectively: $\delta^{65}Cu = [(^{65}Cu/^{63}Cu)_{sample}/(^{65}Cu/^{63}Cu)_{NIST\ 976} - 1] \times 1000$; and $\delta^{i}Zn = [(^{i}Zn/^{64}Zn)^{sample}/(^{i}Zn/^{64}Zn)_{JMC\ 3\text{-}0749L} - 1] \times 1000$, where i refers to 66 or 68. Repeated measurements of the in-house JMC Cu110 and Zn310 solutions yielded average values of 0.00±0.04‰ (2SD) (n = 30) for $\delta^{65}Cu_{110}$ and 0.00 ± 0.07‰ (2SD) (n = 31) for $\delta^{66}Zn_{310}$. The Cu_{NIST} yielded $\delta^{65}Cu_{110} = -0.97 \pm 0.13$‰ (2SD) ($n$ = 27), while the Zn_{Lyon} yielded $\delta^{66}Zn_{310} = -0.10 \pm 0.04$‰ (2SD) ($n$ = 3). Furthermore, IRMM 3702 yielded $\delta^{66}Zn_{310} = -0.41 \pm 0.07$‰ (2SD) ($n$ = 11), which relative to the Zn Lyon gives $\delta^{66}Zn_{Lyon} = -0.31 \pm 0.07$‰ (2SD) ($n$ = 11). This is in excellent agreement with the results of previous studies, e.g., Moeller et al. (2012) and Petit et al. (2008), who reported $\delta^{66}Zn_{Lyon} = -0.29 \pm 0.05$‰ (2SD) ($n$ = 5) and $\delta^{66}Zn_{Lyon} = -0.32 \pm 0.04$‰ (2SD) ($n$ = 4). The details of the analytical

session conditions and the mass bias corrections have been described by Petit et al. (2008) and more recently by Debret et al. (2018).

The Fe isotope analyses were carried out on a Nu Plasma II instrument in dry plasma mode at medium resolution. A DSN-100 desolvator (Nu Instruments, Wrexham, UK) was used for the dry plasma conditions. The solution concentrations for the measurements were 800 µg/L of Fe and 1000 µg/L of Ni in 0.05 M HNO_3. The isotopic ratios were measured ($^{56}Fe/^{54}Fe$ and $^{57}Fe/^{54}Fe$) by applying the sample-standard bracketing method, i.e., using IRMM 014 and external normalization and using Ni as a dopant. The data are reported in delta (δ) notation relative to the IRMM-014 standard (Taylor et al., 1992) and were calculated using the equation $\delta^{i}Fe = [(^{i}Fe/^{54}Fe)_{sample}/(^{i}Fe/^{54}Fe)_{IRMM\text{-}014} - 1] \times 1000$, where i refers to 56 or 57.

The accuracy and precision of the Fe isotope analyses were assured by analyzing reference material IRMM-014 as the bracketing standard and our in-house quality control standard 'MIX'. The mean Fe isotopic compositions of these standards were as follows. IRMM-014: $\delta^{56}Fe = 0.00 \pm 0.07‰$, and $\delta^{57}Fe = 0.01 \pm 0.09‰$ (2SD, $n = 68$). MIX: $\delta^{56}Fe = -1.55 \pm 0.11‰$, and $\delta^{57}Fe = -2.26 \pm 0.16‰$ (2SD, $n = 61$). The long-term averages (2014 to 2016) of the MIX standard are $\delta^{56}Fe = -1.55 \pm 0.10‰$, and $\delta^{57}Fe = -2.28 \pm 0.16‰$ (2SD, $n = 126$).

3. Results

3.1. Major and trace element compositions of MORB

The major element concentrations of the volcanic rocks from the EPR near 13°N and 1–2°S, the CIR, and the SWIR are prsented in Table S5. All the studied volcanic rocks are basalts (SiO_2 = 49.13 − 41.49 wt.%; Na_2O+K_2O =2.54 − 4.66 wt.%) and belong to the low-K arc-tholeiitic series (K_2O = 0.05−0.48 wt.%). The basalts from the SWIR have larger variation ranges of SiO_2 (49.13 − 51.49 wt.%), MgO (6.06 − 8.54 wt.%) and Na_2O (2.43 − 4.28 wt.%) than the basalts from the EPR and SWIR (Table S5). The trace element concentrations of the volcanic rocks from the EPR near 13°N and 1–2°S, the CIR, and the SWIR are presented in Table S6. The primitive mantle normalized spider diagrams of the basalts show obvious depletions of large ion lithophile elements (LILEs) relative to high field strength elements (HFSEs) and rare earth elements (REEs). The chondrite normalized rare earth element (REE) diagrams of the basalts exhibit flat REE distribution patterns (Fig. 2), and the fractionation between the LREEs and HREEs is inconspicuous ($(La/Yb)_N$ = 0.40−1.64). The basalts in this study exhibit insignificant Eu anomalies (δEu = 0.96 − 1.15, $\delta Eu = 2Eu_N/(Sm_N+Gd_N)$) (Fig. 2).

3.2. Fe-Cu-Zn Isotopic Compositions of the MORBs

The Fe, Cu, and Zn isotopic data for the MORB samples are presented in Table 1. The MORBs from the EPR near 13°N, the EPR between 1° and 2°S, the CIR, and the SWIR

exhibit δ^{56}Fe values between +0.06‰ and +0.18‰ (Table 1). The δ^{56}Fe values of the basalt samples from the EPR near 13°N (+0.10 to +0.16‰, avg. +0.127‰, *n* = 6) are similar to those from the EPR between 1° and 2°S (+0.06 to +0.18‰, avg. +0.129‰, *n* = 7) and those from the SWIR (+0.07 to +0.16‰, avg. +0.126‰, *n* = 13) (Table 1). Most of the δ^{56}Fe values of the MORBs (+0.06 to +0.18‰; this study) are within the range of previously studied OIBs (−0.11 to +0.18‰; Beard et al., 2003b; Teng et al., 2013) but are slightly higher than those of previously studied MORBs (+0.07 to +0.14‰: Teng et al., 2013) (Fig. 3).

The measured δ^{65}Cu values of the MORB samples vary from −0.10 to +0.73‰ (Table 1). The δ^{65}Cu values of the basalts from the SWIR exhibit the largest range (−0.10 to +0.73‰; avg +0.30‰, n = 13), with the highest (+0.73‰) and lowest value (−0.10 ± 0.08‰) values of all of the MORB samples (Table 1). With the exception of three basalt samples, which have δ^{65}Cu values (IR05-TVG10-1: −0.01 ± 0.03‰; IR05-TVG3-1: −0.04 ± 0.23‰; and 20YH-S20-TVG17-1: −0.10 ± 0.08‰) that are lower than those of previously studied MORBs (0 to +0.14‰; Liu et al., 2015; Savage et al., 2015), most of the δ^{65}Cu values of the remaining basalt samples are substantially higher than those of previously studied MORBs and OIBs (−0.07 to +0.18‰; Liu et al., 2015; Savage et al., 2015) (Fig. 4).

The measured δ^{66}Zn and δ^{68}Zn values of the basalt samples vary from +0.31 to +0.51‰ and from +0.62 to +1.06‰ (Table 1), respectively, and are higher than those of

previously studied MORBs (δ^{66}Zn of +0.25 to +0.30‰; δ^{68}Zn of +0.53 to +0.60‰; Ben Othman et al., 2006; Wang et al., 2017) and OIBs (δ^{66}Zn of +0.25 to +0.40‰; δ^{68}Zn of +0.50 to +0.79‰; Wang et al., 2017) (Fig. 5). Furthermore, the δ^{66}Zn values of the MORB samples exhibit an increasing trend, from the EPR at 13°N to the EPR between 1° and 2°S to the CIR to the SWIR (Fig. 5).

3.3. Fe-Cu-Zn Isotopic Compositions of the Sulfides

The Fe, Cu, and Zn isotopic data for the MORS and BABS samples are presented in Table 2. The measured δ^{56}Fe and δ^{57}Fe values of the sulfide samples range from −1.96 to +0.11‰ and from −2.89 to +0.19‰, respectively, with no evident relationship between δ^{56}Fe, δ^{57}Fe, and mineral type (pyrite, chalcopyrite, and sphalerite). The δ^{56}Fe values of the pyrite samples from the EPR near 13°N vary between −1.05‰ and −0.29‰ (avg. of −0.66‰, n = 7), which is within the range of the δ^{56}Fe values reported by Rouxel et al. (2008) for pyrite from the EPR between 9°N and 10°N (−1.89 to −0.06‰). The δ^{56}Fe values of the pyrite from the MORS and BABS exhibit a larger range than that of the chalcopyrite (Fig. 3). However, the δ^{56}Fe values of the pyrite samples from the EPR between 1° and 2°S range from −1.74 to −0.01‰ (avg. of −0.77‰, n = 7), while the majority of the δ^{56}Fe values (−0.18 to +0.11‰) of the chalcopyrite are substantially higher than those of the pyrite (Table 2). In the S99HF on the NFB, the δ^{56}Fe value of the chalcopyrite (−0.18 ± 0.05‰) is also substantially higher than those of the pyrite and

sphalerite samples (pyrite: δ^{56}Fe of −1.25 to −0.48‰, avg. of −0.91‰, *n* = 3; sphalerite: δ^{56}Fe of −1.17 to −0.90‰, avg. of −1.02‰, *n* = 4) (Table 2), which places it within the δ^{56}Fe range of the chalcopyrite from the EPR between 9°N and 10°N (−0.33 to −0.11‰; Rouxel et al., 2008). Furthermore, most of the δ^{56}Fe values of the MORS and BABS samples are significantly lower than those of their host MORBs (+0.06 to +0.18‰; Teng et al., 2013; this study) and BABBs (+0.087 to +0.106‰; Teng et al., 2013) (Fig. 3) but are similar to those of the hydrothermal fluids (−1.85 to −0.14‰; *n* = 49; Sharma et al., 2001; Severmann et al., 2004; Rouxel et al., 2008; Moeller et al., 2014).

The measured δ^{65}Cu values of the chalcopyrite vary from −0.88 to −0.16‰. This range is smaller than those of the δ^{56}Fe and δ^{57}Fe values of the MORS and BABS minerals (Table 2) and is lower than those of the host MORBs (δ^{65}Cu of −0.10 to +0.73‰; Liu et al., 2015; Savage et al., 2015; this study) and the hydrothermal fluids (δ^{65}Cu of +0.1 to +0.5‰; Dekov and Rouxel, 2012) (Fig. 4).

The δ^{66}Zn and δ^{68}Zn values of the sphalerite range from −0.39 to −0.03‰ and from −0.77 to −0.03‰ (Table 2), respectively, which is significantly lower than those of their host MORBs (δ^{66}Zn of +0.25 to +0.51‰; this study) and the hydrothermal fluids (δ^{66}Zn of 0.00‰ to +1.33‰; John et al., 2008) but is mostly within the range of seawater (δ^{66}Zn of −0.33 to +0.96‰; Little et al., 2014; Zhao et al., 2014; Samanta et al., 2017) (Fig. 5).

4. Discussion

4.1. Fe-Cu-Zn Isotope Variations in the MORBs

4.1.1 Fe Isotopes

In this study, the δ^{56}Fe values of the MORBs exhibit a narrow range of Fe isotopic compositions (δ^{56}Fe of +0.06 to +0.18‰, avg. of +0.13 ± 0.05‰, *n* = 28). However, the δ^{56}Fe ranges of the MORBs from the EPR at 13°N and 1−2°S, the EHF at CIR, and the A area at SWIR (Table 1; for sample locations, see Table S1) are slightly larger than that of previously studied MORBs (+0.04 to +0.14‰; Weyer & Ionov, 2007; Teng et al., 2013) from the EPR at 13°N, 06°N, 17−19°S, and 21°N; the MAR at 24−36°N, the Kolbeinsey and Knipovich ridges, the Indian Ridge near the Rodriguez Triple Junction and at 39°S, and the Red Sea at 18°N and 20°N (Fig. 3), indicating that slight Fe isotopic fractionation occurred during the melting of the mid-ocean ridge mantle (Weyer and Ionov, 2007; Teng et al., 2013). Moreover, the δ^{56}Fe and δ^{57}Fe values of the MORBs are higher than those of the hydrothermal fluids (δ^{56}Fe of −0.18 to −1.84‰, δ^{57}Fe of −0.20 to −2.71‰; Sharma et al., 2001; Severmann et al., 2004; Rouxel et al., 2008; Moeller et al., 2014) (Fig. 3). This suggests that during the hydrothermal fluid-basalt interactions, the isotopically light Fe may be preferentially incorporated into the hydrothermal fluids, while the isotopically heavy Fe remains in the altered basaltic rocks (Rouxel et al., 2003).

However, several processes and factors that cause variations in the δ^{56}Fe values of volcanic rocks should be considered, including the following four factors: alteration

and/or wall rock assimilation, degree of partial melting, fractional crystallization, and spreading rate (Rouxel et al., 2003; Croal et al., 2004; Anbar et al., 2005; Weyer et al., 2005; Dauphas and Rouxel, 2006; Weyer and Ionov, 2007; Teng et al., 2008; Schuessler et al., 2009; Williams et al., 2009; Hibbert et al., 2012; Weyer and Seitz, 2012; X. Zhao et al., 2012).

1) The studied basalt samples were fresh and unaltered, which is supported by their measured loss on ignition values (0.20% to 0.58%, fresh rocks have low LOI values (<1 %)) (Table S4; Doucet et al., 2016). Therefore, the influences of alteration, wall-rock assimilation and biotic redox processes on the Fe isotopic compositions can be ruled out for the MORBs analyzed in this study.

2) The degree of Fe isotopic fractionation during partial melting is dependent on the degree of partial melting (e.g., the TiO_2 content), the $Fe^{3+}/\sum Fe$ ($\sum Fe = Fe^{3+} + Fe^{2+}$) of the magma source, and the type of melting (buffered versus non-buffered) (Woodhead and Johnson, 1993; Woodhead et al., 1998; Dauphas et al., 2009). However, the variation in their TiO_2 contents is relatively small (1.19 to 1.93 wt.%) (Table S4), and there is no obvious relationship between the $\delta^{56}Fe$ values and TiO_2 contents of the different samples (Fig. S1). Although the estimated $Fe^{3+}/\sum Fe$ ratios of the basalts vary from 0.15 to 0.35, this amount is still considered to be relatively small (Weyer and Ionov, 2007; Teng et al., 2013). Moreover, the range of the degree of partial melting of mantle materials during MORB production varies from 5 to 20% (Christie et al., 1986; Klein and Langmuir, 1987;

Bézos and Humler, 2005; Workman and Hart, 2005; Frost and McCammon, 2008), which alone cannot produce a δ^{56}Fe isotopic variation of more than 0.02‰ (Poitrasson and Freydier, 2005; Schoenberg and von Blanckenburg, 2006; Teng et al., 2008; Dauphas et al., 2009). Thus, partial melting of the mantle cannot fully account for the 0.12‰ variation in the δ^{56}Fe values of the basalts analyzed in this study.

3) The δ^{56}Fe value may increase with the evolution of the fractional crystallization of the magma (i.e., as the SiO_2 content increases) (Poitrasson and Freydier, 2005; Heimann et al., 2008; Schuessler et al., 2009). Petrographic and geochemical studies have demonstrated that olivine and plagioclase are the major fractioning phases in our studied basalt samples. The removal of plagioclase should not affect the melt's Fe isotopic composition since it has a substantially lower FeO content than the residual melt (Teng et al., 2013). Previous studies have suggested that olivine tends to have a light Fe isotopic composition relative to melts (Teng et al., 2008, 2011; Dauphas et al., 2009), and the crystallization of olivine can lead to an increase in the δ^{56}Fe value of the residual melt. However, the olivine contents (a major crystallization phase) of the studied basalt samples are similar, and there is no relationship between their δ^{56}Fe values and SiO_2 contents (Fig. S1), indicating that different amounts of fractional crystallization of olivine and plagioclase cannot explain the variation in the δ^{56}Fe values of the studied basalts (Teng et al., 2008; Dauphas et al., 2009; Schuessler et al., 2009).

4) The spreading rate is a potential factor affecting magmatism at MORs. The 13°N EPR

is a fast-spreading center, with a full spreading rate of 104 mm/a (Bluth and Ohmoto, 1988). The region between 1°S and 2°S on the EPR is an ultrafast spreading ridge segment, with a spreading rate of approximately 150 mm/a (Searle, 1983). The spreading center of the CIR has an intermediate-spreading rate of approximately 48 mm/a in the EHF; Van Dover et al., 2001). The SWIR is an ultraslow-spreading ridge, with a spreading rate of approximately 14 mm/a (Patriat and Segoufin, 1988; DeMets et al., 1994). These ridges and ridge segments constitute the end-members of the global mid-ocean ridge spectrum, providing natural laboratories for testing the potential control exerted by the spreading rate on mantle melting. However, no clear relationship was found between the variations in the Fe isotopic compositions of the basalts from the different ridge segments and the local spreading rates of the ridge segments (Figs. 5a, S2), suggesting that the variation in spreading rate did not significantly affect the Fe isotopic compositions of the basalts.

As was previously discussed, seafloor alteration, partial melting, fractional crystallization, wall-rock assimilation, and mid-ocean ridge spreading rate cannot fully explain the slight variation in the Fe isotopic compositions of the basalts. Moreover, distinct mantle source regions have previously been invoked to explain the elemental (Prytulak and Elliott, 2007; Dasgupta et al., 2010) and radiogenic isotopic (Hofmann, 1997; Workman et al., 2004; Stracke et al., 2005; Salters et al., 2011) signatures of many oceanic basalt suites. This suggests that the clear variation in the Fe isotopic compositions of the basalts in this

study supports the concept of Fe isotopic heterogeneity in the Earth's lithospheric mantle (Rouxel et al., 2003; Teng et al., 2013; Williams & Bizimis, 2014). However, the mid-ocean ridge magma source's Fe isotopic heterogeneity and the different mantle melting processes require further investigation.

4.1.2 Cu Isotopes

The Cu isotopic compositions of the MORB samples exhibit significantly greater variations (−0.10 to +0.73‰, Table 1) than those of previously studied MORBs (0 to +0.14‰; Liu et al., 2015; Savage et al., 2015). These values are also slightly higher than those of previously studied OIBs (−0.07 to +0.18‰; Liu et al., 2015; Savage et al., 2015) (Fig. 4), implying that during melting under the mid-ocean ridge, heavy ^{65}Cu was more likely to be incorporated into the basaltic melt than into the ocean island environment. The rather large range of the Cu isotopic compositions of the studied MORBs is difficult to explain by high-temperature equilibrium Cu isotopic fractionation, such as by partial melting of the mantle, which generates a limited amount Cu isotopic fractionation and is distinct from the behavior of the Fe isotopes, which are significantly fractionated during mantle partial melting (Weyer and Ionov, 2007; Liu et al., 2015). However, mantle metasomatism can produce Cu isotopic fractionation (Fernandez and Borrok, 2009; Liu et al., 2015). Metasomatism in basalts potentially results in sulfide dissolution/breakdown or precipitation (Reisberg et al., 2005). If redox reactions are involved, the released Cu

may be isotopically heavy (Fernandez and Borrok, 2009), leaving the metasomatized basalts isotopically lighter than primary MORBs. In contrast, the precipitation of secondary minerals from fluids that have previously leached Cu from sulfides may enrich the basalts in heavy Cu isotopes. During this process, isotopic fractionation may or may not occur depending on which secondary phase is precipitated. Moreover, the light rare earth elements (LREEs) patterns and the lack of metasomatic minerals can be used to evaluate the effects of metasomatism (Zheng et al., 2005; Chu et al., 2009; Liu et al., 2015; Zhao et al., 2015). The metasomatized basalts exhibit LREE-enriched patterns ($(La/Sm)_N$ >1) and commonly contain metasomatic products (e.g., phlogopite), whereas the non-metasomatized basalts display LREE-depleted or flat rare earth element patterns and lack visible metasomatic minerals (Liu et al., 2015). Moreover, evidence of metasomatism was not observed in most of the studied samples ($(La/Sm)_N$ = 0.41–0.98, avg. of 0.66, *n* = 22, except for samples 20III-S10-TVG7 and IR05-TVG4-1) (Fig. S3). Thus, the influence of metasomatism on the variation in the Cu isotopic compositions of the basalts can be ruled out. However, samples 20III-S10-TVG7 and IR05-TVG4-1, which have $(La/Sm)_N$ >1 (1.21 and 1.01, respectively) and higher δ^{65}Cu values (0.55‰ and 0.69‰, respectively) than the other studied samples, can be explained by the influence of metasomatism via melt/fluid-rock interactions (Fernandez and Borrok, 2009; Liu et al., 2015).

Similar to the δ^{56}Fe variability, one explanation for the relatively large variation in the

δ^{65}Cu values of the basalt samples is that they were derived from Earth's δ^{65}Cu-heterogeneous lithospheric mantle (Savage et al., 2014; Liu et al., 2015). This also implies that the varied Cu isotopic compositions of the studied MORBs may result from the δ^{65}Cu heterogeneity of their mantle sources.

4.1.3 Zn Isotopes

The Zn isotopic values of the studied MORB samples range from +0.31 to +0.51‰, which significantly exceeds the δ^{66}Zn range of previously reported MORBs (+0.26 to +0.30‰; Wang et al., 2017) and is higher on average than those of previously studied OIBs (+0.25 to +0.40‰; Ben Othman et al., 2006; Wang et al., 2017) (Fig. 5). This implies that the magma evolution processes may have caused Zn isotopic fractionation, and during melting under the mid-ocean ridge, heavy ^{66}Zn and ^{68}Zn were more likely to be incorporated into the basaltic melt than into the ocean island environment (Ben Othman et al., 2006; Wang et al., 2017).

However, the sedimentary carbonates exhibit substantially heavier Zn isotopic compositions (up to +1.34‰; Pichat et al., 2003; Kunzmann et al., 2013) compared to the studied MORBs (+0.31 to +0.51‰), and the recycling of sedimentary carbonates into the mantle may result in elevated δ^{66}Zn values, which has been observed in continental basalts in eastern China (Liu et al., 2016). Moreover, certain highly evolved silica-rich rocks (e.g., pegmatites) may exhibit high δ^{66}Zn values (+0.53 to +0.88‰; Telus et al.,

2012), and mantle metasomatism processes may cause significant Zn isotopic variations in mantle rocks (Wang et al., 2017). Therefore, metasomatism by silica-rich melts may be responsible for the heavier δ^{66}Zn values of the basalts. However, the studied basalt samples, which were recovered from a mid-ocean ridge tectonic setting with mafic/ultramafic magma, were the major host magmas, and the addition of sedimentary carbonates and silica-rich rocks to the magma source is unlikely. Moreover, Zn is a monovalent element (Lodders, 2003); and thus, isotope fractionation induced by a change in oxidation state can be excluded (Wang et al., 2017). Fractional crystallization of basaltic magmas and mantle partial melting are other possible mechanisms that could cause the differences in the Zn isotopic compositions of the basalts and the mantle magma (Wang et al., 2017). Moreover, fractional crystallization has been proposed to explain the Zn isotopic variations observed in the Kilauea Iki lavas (Chen et al., 2013). The basalt with an isotopically heavier Zn composition was thought to undergo fractionation of olivine and Fe–Ti oxides, whereas the basalts with the lightest δ^{66}Zn values were interpreted to be the result of olivine and chromite accumulation (Chen et al., 2013). Furthermore, experimental studies have demonstrated that spinel is one of the major Zn hosts in basaltic magma (Le Roux et al., 2011; Davis et al., 2013), and it is isotopically heavier than other coexisting silicate minerals (Ol, Cpx, and Opx) (Wang et al., 2017). Therefore, the preferential melting of spinel is another likely mechanism of Zn isotopic fractionation, and the δ^{66}Zn values of the residual melt become lighter once the

spinel is exhausted. That is, the melts become isotopically heavier as larger amounts of spinel are incorporated into the melts, until complete melting of the spinel occurs. Thus, spinel melting is a reasonable mechanism for the Zn isotopic fractionation produced during partial melting of the mantle (Wang et al., 2017).

However, as previously discussed, olivine and plagioclase are the major fractionating phases, and the degrees of partial melting of the studied basalt samples are similar. Chen et al. (2013) found that fractional crystallization causes only very limited (≤0.1‰) Zn isotopic fractionation between lavas and their related cumulates. Therefore, it appears that fractional crystallization and/or the degree of partial melting of the mantle cannot explain the large variations in the Zn isotopic composition of our samples.

However, mantle heterogeneity has been suggested as a potential cause of Zn isotopic fractionation. This phenomenon has been used to explain the distinctly different Zn isotopic compositions of fertile lherzolites and refractory spinel harzburgites (Ionov et al., 2010; Chen et al., 2013; Doucet et al., 2016). This suggests that Earth's heterogeneous lithospheric mantle may be a major cause of the distinct variation in the δ^{66}Zn values of our basalts.

It is interesting that the studied samples not only exhibit heterogeneous isotopic compositions, but there is a generally increasing trend in the δ^{66}Zn values of the MORBs from the EPR to the CIR to the SWIR (Fig. 6c). This, coupled with the different mid-ocean ridge spreading rates, suggests that ^{66}Zn and ^{68}Zn are more likely to be

incorporated into the basaltic magma under the ultra-slow-spreading SWIR than into that under the fast-spreading EPR. Therefore, the variation in the mid-ocean ridge spreading rates can explain the variations in the Zn isotopic values of the different mid-ocean ridge tectonic settings. This implies that a faster spreading rate may result in lighter Zn isotopic values, i.e., closer to a MORB-like Zn isotopic composition.

4.2. Fe-Cu-Zn Isotopic Variations in the MORS and BABB

4.2.1 Fe Isotopes

It is well known that the hydrothermal activity on the EPR near 13°N, on the EPR between 1°S and 2°S, in the EHF on the CLR, and in A area on the SWIR are hosted by MORBs, while that in the S99HF on the NFB is hosted by BABBs (Zeng et al., 2010, 2014, 2015a, 2015b, 2017). The Fe isotopic compositions of the hydrothermal fluids (−1.85 to −0.14‰; Sharma et al., 2001; Severmann et al., 2004; Rouxel et al., 2008; Moeller et al., 2014) (Fig. 3) differ significantly from the Fe isotopic compositions (+0.06 to +0.18‰; Teng et al., 2013; this study) of the MORBs and BABBs, which are substantially lower than those of the host basalts (+0.06 to +0.18‰; Teng et al., 2013; this study). Therefore, the Fe isotopic compositions of sulfides can be used as evidence to determine the diagnostic isotopic signature of the Fe released into the oceans by seafloor hydrothermal vents and the interactions between the various Fe reservoirs (Severmann et al., 2004).

The δ^{56}Fe values of the MORS and BABS minerals range from −1.96 to +0.11‰ (Table 2), which are significantly lower than those of their host basalts (+0.06 to +0.18‰; Teng et al., 2013; this study) (Fig. 3) and are generally similar to the δ^{56}Fe values of hydrothermal fluids (−1.85 to −0.14‰; Sharma et al., 2001; Severmann et al., 2004; Rouxel et al., 2008; Moeller et al., 2014) (Fig. 3). This indicates that the hydrothermal fluids are a source of the Fe in the sulfide minerals, and the ^{54}Fe in their host MORBs and BABBs is more likely to be incorporated into the fluids during fluid-basalt interactions. Thus, it has been suggested that hydrothermal fluids also provide a source of light Fe isotopes to the deep oceans (Sharma et al., 2001; Severmann et al., 2004; Rouxel et al., 2008; Bennett et al., 2009; Moeller et al., 2014), and the interactions between the host basalt and the fluids result in the preferential leaching of lighter Fe isotopes from the hydrothermally altered basaltic rocks, while the heavier Fe isotopes remain behind in the altered oceanic crust (Polyakov and Mineev, 2000; Bullen et al., 2001; Schauble et al., 2001; Sharma et al., 2001, Johnson et al., 2002, 2003; Rouxel et al., 2003). This implies that a plate subduction component containing altered rocks (with heavier Fe isotopic compositions) has an influence on the back-arc basin and island arc magma sources, thereby resulting in the preferential enrichment of heavier Fe isotopes in back-arc basin and island arc volcanic rocks.

The chalcopyrite has a limited range of δ^{56}Fe values between −0.18‰ and +0.11‰, indicating a small amount of Fe isotopic fractionation (up to 0.3‰) between the host

basalts (+0.06 to +0.18‰) and the vent fluids (−1.85 to −0.14‰) (Fig. 3). This suggests that the Fe in the chalcopyrite was derived from the interactions between the hydrothermal fluids and the host basalt. As was previously observed by Rouxel et al. (2008), in the hydrothermal field on the EPR between 9°N and 10°N, the δ^{56}Fe values of the chalcopyrite tend to be systematically more positive compared to those of the coexisting pyrite and sphalerite (Table 2, Fig. 7a), suggesting that a small amount of positive Fe isotopic fractionation occurs during chalcopyrite precipitation.

We also observed this phenomenon on the EPR between 1°S and 2°S, in the EHF on the CIR, and in the S99HF on the NFB, where the δ^{56}Fe and δ^{57}Fe values of the chalcopyrite are significantly higher than those of the coexisting pyrite and sphalerite (Table 2, Fig. 7a). This suggests that the Fe isotopes of the sulfides and fluids are in disequilibrium (Sharma et al., 2001; Rouxel et al., 2008), and that ^{56}Fe and ^{57}Fe are more likely to be incorporated into chalcopyrite under high-temperature fluid conditions (Butler and Nesbitt, 1999). Thus, the high-temperature chalcopyrite is characterized by enriched δ^{56}Fe and δ^{57}Fe values (Fig. 7a). Furthermore, the δ^{56}Fe values (+0.11 ± 0.09‰) of the chalcopyrite from the hydrothermal field on the EPR between 1°S and 2°S are close to those of their host basalts (+0.06 to +0.18‰). This indicates that the Fe was mainly leached from the local basaltic rocks and was incorporated into the chalcopyrite under high-temperature fluid conditions. Moreover, this means that no significant Fe isotopic fractionation occurred during the high-temperature basalt-fluid interactions.

The δ^{56}Fe values of the pyrite exhibit a large variation (−1.96 to +0.11‰) compared to those of the host basaltic rocks (+0.06 to +0.18‰), with a large amount of Fe isotopic fractionation (up to 2‰). This is consistent with the varying fluid temperatures, which ranged from high to low during the pyrite formation (Fig. 7a) (Abraitis et al., 2004; Keith et al., 2016). These values are slightly lower than the δ^{56}Fe values of seawater (−0.88 to +0.10‰; Rouxel and Maureen, 2010) and are similar to the δ^{56}Fe values of hydrothermal fluids (−1.85 to −0.14‰; Sharma et al., 2001; Severmann et al., 2004; Rouxel et al., 2008; Moeller et al., 2014) (Fig. 3). All these findings indicate that the fluids may be a source of the light Fe isotopic compositions of the sulfides, and that ^{54}Fe is more likely to be preferentially incorporated into pyrite facies during mixing between seawater and hydrothermal fluids. This suggests that low-temperature pyrite is characterized by depleted δ^{56}Fe and δ^{57}Fe values (Fig. 7a).

Rouxel et al. (2008) reported that the relatively slow precipitation of pyrite in subsurface environments due to conductive cooling of the fluids produces limited Fe isotopic fractionation, while the rapid precipitation of pyrite as a result of mixing in chimney environments produces significant kinetic Fe isotopic fractionation. Therefore, the large variation in the Fe isotopic compositions of the sulfide minerals is likely to have been influenced by the precipitation rate. The Fe isotope results reveal that the chalcopyrite has systematically higher δ^{56}Fe values than the pyrite and sphalerite (Fig. 3), which means that the pyrite, sphalerite, and chalcopyrite within a single hydrothermal field exhibit Fe

isotope disequilibrium. Moreover, there is no clear relationship between the Fe isotopic compositions of the sulfides from the different ridge segments and the local mid-ocean ridge spreading rates (Figs. 5a, S2), suggesting that the mid-ocean ridge spreading rate did not significantly affect the Fe isotopic compositions of the sulfide minerals in the local hydrothermal fields.

Furthermore, the sphalerite minerals from the EHF on the CIR and the S99HF on the NFB include small amounts of pyrite and chalcopyrite, and the δ^{56}Fe values of the sphalerite minerals from the EHF on the CIR and the S99HF on the NFB exhibit large variations (−1.65 to −0.63‰) compared to those of the chalcopyrite (Fig. 3), implying that the Fe isotopic compositions of the sphalerite are controlled by small pyrite and chalcopyrite inclusions, which can be used to trace the sulfide inclusions in the sphalerite.

4.2.2 Cu Isotopes

The chalcopyrite from the sulfide samples have consistently depleted δ^{65}Cu values, with a smaller δ^{65}Cu range (−0.88 to −0.16‰) than that of the Fe isotopes of the sulfide minerals. They also exhibit a small amount of Cu isotopic fractionation (up to 0.7‰), which is significantly lower than that of the host MORBs and the hydrothermal fluids (Fig. 4). This suggests that ^{63}Cu was preferentially removed from the hydrothermal fluids and was incorporated into the chalcopyrite during the formation of the chalcopyrite, while the heavier Cu isotope was more likely to remain in the high-temperature fluids

from which the chalcopyrite precipitated (Fig. 7b). This implies that the hydrothermal fluids, which have heavier Cu isotopic compositions, may provide a source of heavy Cu isotopes to hydrothermal plumes, seawater, and metalliferous sediments during fluid-seawater mixing and the settling of hydrothermal materials.

This is consistent with the general observations of Zhu et al. (2000) regarding the EPR hydrothermal fields, in which the inactive sulfide deposits have more depleted δ^{65}Cu values than the active high-temperature hydrothermal vents, which have significantly lower values than the host MORBs (avg. of +0.07 ± 0.06‰; Liu et al., 2015; Savage et al., 2015; this study) and the hydrothermal fluids (+0.1 to +0.5‰; Dekov and Rouxel, 2012) (Fig. 4). This suggests that the Cu isotopes of the chalcopyrite and the hydrothermal fluids are in disequilibrium, and that significant Cu isotopic fractionation occurred between the chalcopyrite and the hydrothermal fluids. This can be explained by the Cu isotopic exchange that occurs during redox processes and the precipitation of chalcopyrite. Furthermore, the hydrothermal processes did not lead to a large amount of Cu isotopic fractionation in the chalcopyrite, suggesting that direct precipitation in equilibrium with the end-member fluids produces positive Cu isotopic compositions, as opposed to the observed negative Cu isotopic compositions of the chalcopyrite.

However, sulfides that are crystallized during early stage hydrothermal processes are known to undergo extensive chemical and textural modifications during subsequent hydrothermal diagenesis (Sharma et al., 2001; Rouxel et al., 2004b, 2008). This may lead

to reactions between the δ^{65}Cu-depleted, late-stage fluids and the earlier-formed sulfides to produce the δ^{65}Cu-depleted sulfides (Zhu et al., 2000). Rouxel et al. (2004b) reported that hydrothermal sulfides characterized by negative δ^{65}Cu values have undergone extensive recrystallization. If heavy Cu isotopes are released during the reworking and/or alteration of chalcopyrite, the δ^{65}Cu values of the residual sulfides should become more negative as the replacement reactions proceed (Rouxel et al., 2004b). Therefore, the negative δ^{65}Cu values of the chalcopyrite from the sulfide samples in this study may be the product of replacement recrystallization via a reaction with later δ^{65}Cu-depleted fluids. This suggests that the ^{63}Cu in the hydrothermal fluids is more likely to be incorporated into the chalcopyrite facies during replacement recrystallization, and the Cu isotopic compositions of the sulfides can be used to decipher the details of seafloor hydrothermal redox processes. Furthermore, the mid-ocean ridge segments from which our hydrothermal sulfide samples were collected are sediment starved, making the incorporation of significant amounts of Cu originating from a sedimentary source unlikely. Moreover, seawater exhibits a large range of heavier Cu isotopic compositions (−0.18 to +1.44‰; Vance et al., 2008; Little et al., 2014) compared to the chalcopyrite in this study (Fig. 4). The Cu concentration of seawater is approximately 2×10^{-9} mol/kg (Wu and Boyle, 1997), which is significantly lower than that of high-temperature hydrothermal fluids ($9.7–150 \times 10^{-6}$ mol/kg; Edmond et al., 1996; Elderfield and Schultz, 1996). Therefore, mixing between seawater and hydrothermal fluids or the mantle source

cannot explain the observed negative Cu isotopic compositions of the studied hydrothermal sulfides.

4.2.3 Zn Isotopes

In hydrothermal systems, Zn isotopes can also be used as tracers of seafloor hydrothermal processes, thereby increasing our understanding of the plumbing and chemistry of hydrothermal vents (John et al., 2008). Possible Zn isotopic fractionation and the magnitude thereof should be considered prior to evaluating the potential of using Zn isotopes to trace the source of ore-forming metals. Several processes are considered to be potential causes of Zn isotope variations during ore-forming processes, including: (1) temperature effects (Mason et al., 2005; Toutain et al., 2008), (2) the mixing of multiple zinc sources (Wilkinson et al., 2005; Zhou et al., 2014), and/or (3) kinetic Raleigh fractionation during mineral precipitation (Kelley et al., 2009; Gagnevin et al., 2012). The δ^{66}Zn values of the sphalerite (−0.39 to −0.03‰) in this study are substantially lower than those of the host basalts (>0.31‰, Table 1) and the hydrothermal fluids (+0.00 to +1.04‰; John et al., 2008), which are in the range of seawater (Fig. 5) (−0.33 to +0.80‰; Little et al., 2014; Zhao et al., 2014; Samanta et al., 2017). This suggests that the Zn isotopes of the sphalerite and the hydrothermal fluids are in disequilibrium. Significant Zn isotopic fractionation occurred between the sphalerite and the hydrothermal fluids due to the Zn isotopic exchange during fluid-seawater mixing and sphalerite precipitation.

However, the ^{64}Zn in the hydrothermal fluids was more likely to be incorporated into the sphalerite during the mixing of the seawater and hydrothermal fluids, resulting in the hydrothermal fluids from which the sphalerite precipitated being preferentially enriched in the heavier Zn isotopes (Dekov and Rouxel, 2012).

This suggests that fluids with heavier Zn isotopic compositions can provide a source of heavy Zn isotopes to hydrothermal plumes, seawater, and metalliferous sediments during fluid-seawater mixing and the settling of hydrothermal materials. Furthermore, equilibrium isotopic fractionation is a function of temperature, with larger amounts of fractionation occurring at lower temperatures (Urey, 1947). The experimental studies conducted by Maréchal and Sheppard (2002) demonstrated that limited Zn isotope variation occurs within a temperature range of 30–50°C. The fluid temperatures in the EHF and NFB are 273–382°C (Gallant and Von Damm, 2006) and 285–291°C (Grimaud et al., 1991; Ishibashi et al., 1994a, 1994b), respectively. These results indicate that the deposition of the Zn in the sphalerite carried ^{66}Zn and ^{68}Zn out of the host basalts during the fluid-basalt interactions under medium- and/or low-temperature fluid conditions (Fig. 7c), resulting in the preferential enrichment of the hydrothermally altered basaltic rocks in the lighter Zn isotopes during the host basalt-fluid interactions. This implies that the influence of a plate subduction component containing altered rocks on the magma source results in the preferential enrichment of back-arc basin and island arc volcanic rocks in the lighter Zn isotope. Furthermore, the δ^{66}Zn values of MORBs are slightly higher than

those of OIBs (Fig. 5), implying that the isotopic heterogeneity of OIBs (Herzog et al., 2009; Teng et al., 2013) may be explained by hydrothermally altered oceanic crust with lower δ^{66}Zn values being injected into the OIB magma.

However, Rayleigh distillation can fractionate Zn isotopes in hydrothermal fluids, with δ^{66}Zn values increasing from the early to late stages due to the precipitation of ^{64}Zn-enriched sulfides (such as sphalerite). John et al. (2008) reported that the subsurface precipitation of isotopically light Zn sulfides is the main cause of the isotopic variations in hydrothermal fluids. Moreover, several studies have identified or inferred the preferential incorporation of lighter Zn isotopes into Zn sulfide precipitates (e.g., Wilkinson et al., 2005), and laboratory experiments have also demonstrated that sulfide precipitation is accompanied by isotopic effects (i.e., Δ^{66}Zn = −0.36‰; Archer et al., 2004). Therefore, during the evolution of hydrothermal fluids, the precipitation of sulfides may cause Zn isotopic fractionation, with the minerals being enriched in light Zn isotopes and the hydrothermal fluid being enriched in heavy Zn isotopes. Theoretical calculations indicate that the Zn isotopic fractionation between an aqueous Zn solution and a sulfide species is 0.2‰ at approximately 300°C (Fujii et al., 2011). However, when Zn isotopic fractionation between hydrothermal fluids and sulfides (0.2‰) is considered (Fujii et al., 2011), the δ^{66}Zn values of the hydrothermal fluids were calculated to be −0.06‰ and 0.00‰ for the EHF and S99HF, respectively. These values are lower than the measured δ^{66}Zn values of the hydrothermal fluids (0.00 to +1.33‰; John et al., 2008),

implying that other sources with low $\delta^{66}Zn$ values were involved. According to Figure 5, seawater with low $\delta^{66}Zn$ values (−0.33 to +0.96‰; Little et al., 2014; Y. Zhao et al., 2014; Samanta et al., 2017) may be a suitable candidate to explain the low $\delta^{66}Zn$ values of the sphalerite. When hydrothermal fluids mix with seawater, additional isotopically light Zn is incorporated into the sulfide precipitates, which could account for the low $\delta^{66}Zn$ values of the sphalerite from the EHF and S99HF obtained in this study.

5. Conclusions

The Fe, Cu, and Zn isotopic compositions of the MORBs analyzed in this study exhibit various $\delta^{56}Fe$ (+0.06 to +0.18‰), $\delta^{65}Cu$ (−0.10 to +0.73‰), and $\delta^{66}Zn$ (+0.31 to +0.51‰) ranges, which are beyond the ranges of previously studied MORBs. The $\delta^{66}Zn$ values of the MORBs are slightly higher than those of the OIBs due to the incorporation of hydrothermally altered oceanic crust into the OIB magma. However, unlike the Fe and Cu isotopes, the $\delta^{66}Zn$ values of the basalts exhibit an increasing trend from the fast-spreading EPR to the intermediate-spreading CIR to the ultraslow-spreading SWIR, suggesting that ^{66}Zn is more likely to be incorporated into the basaltic magma under an ultraslow-spreading mid-ocean ridge, despite the fact that the Zn isotopic composition of the mid-ocean ridge mantle is heterogeneous. Furthermore, no relationship between the variations in the Fe and Cu isotopic compositions of the MORBs from the different ridge

segments and the local spreading rates was identified, suggesting that the mid-ocean ridge spreading rate and the magmatic processes did not affect the Fe and Cu isotopic compositions of the MORBs. As with the Zn isotopic compositions, the varied Fe and Cu isotopic compositions of the studied MORBs could have resulted from the δ^{56}Fe and δ^{65}Cu heterogeneities of the mantle sources.

The δ^{56}Fe values of the MORS and BABS vary from −1.96 to +0.11‰, which is within the range of the hydrothermal fluids but is significantly lower than those of the host MORBs and BABBs, suggesting that the hydrothermal fluids could be a major source of the negative Fe isotopic compositions of the sulfides. However, Fe isotopic fractionation of up to 2‰ was observed for pyrite precipitated from high to low temperature hydrothermal fluids, and the majority of the δ^{56}Fe and δ^{57}Fe values of the chalcopyrite are higher than those of the sphalerite and pyrite. This indicates that the high-temperature sulfides are characterized by enriched δ^{56}Fe and δ^{57}Fe values, while the medium- and low-temperature sulfides are characterized by depleted δ^{56}Fe and δ^{57}Fe values.

The chalcopyrite from the MORS and BABS have a smaller range of δ^{65}Cu values (−0.88 to −0.16‰) and exhibit less Cu isotopic fractionation (up to 0.7‰). These values are significantly lower than those of their host MORBs and hydrothermal fluids, suggesting the preferential enrichment of the hydrothermal fluids from which the chalcopyrite precipitated in heavier Cu isotopes.

The sphalerite in the MORS and BABS exhibit a small range of δ^{66}Zn values (−0.39 to

−0.03‰), with a small amount of Zn isotopic fractionation (up to 0.3‰). These values are also significantly lower than those of the host MORBs and hydrothermal fluids, which are within the range of seawater, suggesting that the Zn deposition during the sphalerite precipitation carried ^{64}Zn out of the hydrothermal fluids during seawater-hydrothermal fluid mixing under medium- and/or low-temperature conditions. The ^{54}Fe in the basalts was more likely to be incorporated into the hydrothermal fluids during the fluid-basalt interactions, while the ^{64}Zn in the hydrothermal fluids was more likely to be incorporated into the sphalerite during seawater-hydrothermal fluid mixing. This resulted in the preferential enrichment of the heavier Zn isotopes in the fluids and thus the heavier Fe and lighter Zn isotopic compositions of the altered rocks. This implies that the influence of a plate subduction component containing hydrothermally altered rocks on the back-arc basin and island arc magma sources results in the preferential enrichment of heavier Fe and lighter Zn isotopes in back-arc basin and island arc volcanic rocks.

It is possible that hydrothermal fluids with heavier Cu and Zn isotopic compositions result in the preferential enrichment of heavier Cu and Zn isotopes in hydrothermal plumes, seawater, and metalliferous sediments during fluid-seawater mixing and the settling of hydrothermal materials. Moreover, the Cu and Zn isotopes of the sulfides and the hydrothermal fluids are in disequilibrium, which can be explained by isotopic exchange during the precipitation of chalcopyrite and sphalerite. Furthermore, significant

Cu and Zn isotopic fractionation occurred between the hydrothermal fluids and the precipitated sulfide minerals, and the redox processes, hydrothermal fluid-seawater mixing, and sulfide precipitation likely caused the Cu and Zn isotopic fractionation. Our findings improve our understanding of the Fe, Cu, and Zn isotopic compositions of sulfides and volcanic rocks as well as the mechanisms responsible for these compositions.

Data Availability

All of the data generated and/or analyzed during this study are available from the corresponding author upon reasonable request.

Acknowledgements

We would like to thank the crews of the DY105-17, DY115-19, DY115-20, and DY115-21 cruises for their help with the sample collection. We are grateful to Dr. Erio Rahders of the Institute for Geological Sciences, Geology Department, Free University of Berlin, and Dr. Huaiming Li of the Second Institute of Oceanography, State Oceanic Administration, China, for providing some of the samples. This research was supported by the National Natural Science Foundation of China (91958213), the Strategic Priority Research Program of the Chinese Academy of Sciences (XDB42020402), the National Program on Global Change and Air-Sea Interaction (GASI-GEOGE-02), the International

Partnership Program of the Chinese Academy of Sciences (133137KYSB20170003), the Taishan Scholar Foundation of Shandong Province (ts201511061), the National Special Fund for the 13th Five Year Plan of COMRA (DY135-G2-01-02), and the National Key Basic Research Program of China (2013CB429700). We thank LetPub for its linguistic assistance during the preparation of this manuscript.

Declaration of Interest Statement

All authors of this manuscript have directly participated in planning, execution, and/or analysis of this study. The contents of this manuscript have not been copyrighted or published previously. The contents of this manuscript are not now under consideration for publication elsewhere. The contents of this manuscript will not be copyrighted, submitted, or published elsewhere while acceptance by Marine Geology.

We declare that we have no financial and personal relationships with other people or organizations that can inappropriately influence our work, there is no professional or other personal interest of any nature or kind in any product, service and/or company that could be construed as influencing the position presented in, or the review of, the manuscript entitled.

References

Abraitis, P. K., Pattrick, R. A. D., Vaughan, D. J., 2004. Variations in the compositional, textural and electrical properties of natural pyrite: a review. *Int. J. Miner. Process.* *74*(1–4), 41–59. https://dx.doi.org/10.1016/j.minpro.2003.09.002

Anbar, A. D., Jarzecki, A. A., Spiro, T. G., 2005. Theoretical investigation of iron isotope fractionation between $Fe(H_2O)_6^{3+}$ and $Fe(H_2O)_6^{2+}$: implications for iron stable

isotope geochemistry. *Geochim. Cosmochim. Acta 69*(4), 825–837. https://dx.doi.org/10.1016/j.gca.2004.06.012

Archer, C., Vance, D., 2004. Mass discrimination correction in multiple-collector plasma source mass spectrometry: an example using Cu and Zn isotopes. *J. Anal. At. Spectrom. 19*(5), 656–665. https://dx.doi.org/10.1039/b315853e

Beard, B. L., Johnson, C. M., Von Damm, K. L., Poulson, R. L., 2003a. Iron isotope constraints on Fe cycling and mass balance in oxygenated Earth oceans. *Geology, 31*(7), 629–632. https://dx.doi.org/10.1130/0091-7613(2003)031<0629:iicofc>2.0.co;2

Beard, B. L., Johnson, C. M., Skulan, J. L., Nealson, K. H., Cox, L., Sun, H., 2003b. Application of Fe isotopes to tracing the geochemical and biological cycling of Fe. *Chem. Geol. 195*(1–4), 87–117. https://dx.doi.org/10.1016/s0009-2541(02)00390-x

Bennett, S. A., Rouxel, O., Schmidt, K., Garbe-Schönberg, D., Statham, P. J., German, C. R., 2009. Iron isotope fractionation in a buoyant hydrothermal plume, 5°S Mid-Atlantic Ridge. *Geochim. Cosmochim. Acta 73*(19), 5619–5634. https://dx.doi.org/10.1016/j.gca.2009.06.027

Ben Othman, D., Luck, J. M., Bodinier, J. L., Arndt, N. T., Albarède, F., 2006. Cu–Zn isotopic variations in the Earth's mantle. *Geochim. Cosmochim. Acta 70*(S18), A46. https://dx.doi.org/10.1016/j.gca.2006.06.201

Bézos, A., Humler, E., 2005. The $Fe^{3+}/\Sigma Fe$ ratios of MORB glasses and their implications for mantle melting. *Geochim. Cosmochim. Acta 69*(3), 711–725. https://dx.doi.org/10.1016/j.gca.2004.07.026

Bluth, G. J., Ohmoto, H., 1988. Sulfide-sulfate chimneys on the East Pacific Rise, 11 degrees and 13 degrees N latitudes; Part II, sulfur isotopes. *Can. Mineral. 26*(3), 505–515.

Bowers, T. S., Campbell, A. C., Measures, C. I., Spivack, A. J., Khadem, M., Edmond, J. M., 1988. Chemical controls on the composition of vent fluids at 13°–11°N and 21°N, East Pacific Rise. *J. Geophys. Res. Solid Earth 93*(B5), 4522–4536. https://dx.doi.org/10.1029/jb093ib05p04522

Bullen, T. D., White, A. F., Childs, C. W., Vivit, D. V., Schulz, M. S., 2001. Demonstration of significant abiotic iron isotope fractionation in nature. *Geology, 29*(8), 699–702. https://dx.doi.org/10.1130/0091-7613(2001)029<0699:dosaii>2.0.co;2

Butler, I. B., Nesbitt, R. W., 1999. Trace element distributions in the chalcopyrite wall of a black smoker chimney: insights from laser ablation inductively coupled plasma mass spectrometry (LA–ICP–MS). *Earth Planet. Sci. Lett. 167*(3–4), 335–345. https://dx.doi.org/10.1016/s0012-821x(99)00038-2

Chen, H., Savage, P. S., Teng, F. Z., Helz, R. T., Moynier, F., 2013. Zinc isotope fractionation during magmatic differentiation and the isotopic composition of the

bulk Earth. *Earth Planet. Sci. Lett. 369–370*, 34–42. https://dx.doi.org/10.1016/j.epsl.2013.02.037

Christie, D. M., Carmichael, I. S. E., Langmuir, C. H., 1986. Oxidation states of mid-ocean ridge basalt glasses. *Earth Planet. Sci. Lett. 79*(3–4), 397–411. https://dx.doi.org/10.1016/0012-821x(86)90195-0

Chu, N. C., Johnson, C. M., Beard, B. L., German, C. R., Nesbitt, R. W., Frank, M., Bohn, M., Kubik, P. W., Usui, A., Graham, I., 2006. Evidence for hydrothermal venting in Fe isotope compositions of the deep Pacific Ocean through time. *Earth Planet. Sci. Lett. 245*(1–2), 202–217. https://dx.doi.org/10.1016/j.epsl.2006.02.043

Chu, Z. Y., Wu, F. Y., Walker, R. J., Rudnick, R. L., Pitcher, L., Puchtel, I. S., Yang, Y. -H., Wilde, S. A., 2009. Temporal evolution of the lithospheric mantle beneath the eastern North China Craton. *J. Petrol. 50*(10), 1857–1898. https://dx.doi.org/10.1093/petrology/egp055

Croal, L. R., Johnson, C. M., Beard, B. L., Newman, D. K., 2004. Iron isotope fractionation by Fe(II)-oxidizing photoautotrophic bacteria. *Geochim. Cosmochim. Acta 68*(6), 1227–1242. https://dx.doi.org/10.1016/j.gca.2003.09.011

Dasgupta, R., Jackson, M. G., Lee, C. T. A., 2010. Major element chemistry of ocean island basalts—conditions of mantle melting and heterogeneity of mantle source.

Earth Planet. Sci. Lett. 289(3–4), 377–392. https://dx.doi.org/10.1016/j.epsl.2009.11.027

Dauphas, N., Rouxel, O., 2006. Mass spectrometry and natural variations of iron isotopes. *Mass Spectrom. Rev. 25*(4), 515–550. https://dx.doi.org/10.1002/mas.20078

Dauphas, N., Craddock, P. R., Asimow, P. D., Bennett, V. C., Nutman, A. P., Ohnenstetter, D., 2009. Iron isotopes may reveal the redox conditions of mantle melting from Archean to present. *Earth Planet. Sci. Lett. 288*(1–2), 255–267. https://dx.doi.org/10.1016/j.epsl.2009.09.029

Davis, F. A., Humayun, M., Hirschmann, M. M., Cooper, R. S., 2013. Experimentally determined mineral/melt partitioning of first-row transition elements (FRTE) during partial melting of peridotite at 3GPa. *Geochim. Cosmochim. Acta 104*, 232–260. https://dx.doi.org/10.1016/j.gca.2012.11.009

Debret, B., Beunon, H., Mattielli, N., Andreani, M., Ribeiro da Costa, I., Escartin, J., 2018. Ore component mobility, transport and mineralization at mid-oceanic ridges: a stable isotopes (Zn, Cu and Fe) study of the Rainbow massif (Mid-Atlantic Ridge 36°14′N). *Earth Planet. Sci. Lett. 503*, 170–180. https://dx.doi.org/10.1016/j.epsl.2018.09.009

Dekov, V., Rouxel, O., 2012. *Cu- and Zn-isotope systematics of seafloor hydrothermal vent fluids from a back-arc setting (Manus Basin)*. Paper presented at EGU General Assembly 2012, European Geosciences Union, Vienna, Austria.

DeMets, C., Gordon, R. G., Argus, D. F., Stein, S., 1994. Effect of recent revisions to the geomagnetic reversal time scale on estimates of current plate motions. *Geophys. Res. Lett. 21*(20), 2191–2194. https://dx.doi.org/10.1029/94gl02118

Doe, B. R., 1994. Zinc, copper, and lead in mid-ocean ridge basalts and the source rock control on Zn/Pb in ocean-ridge hydrothermal deposits. *Geochim. Cosmochim. Acta* 58(10), 2215 – 2223.

Doucet, L. S., Mattielli, N., Ionov, D. A., Debouge, W., Golovin, A. V., 2016. Zn isotopic heterogeneity in the mantle: a melting control? *Earth Planet. Sci. Lett. 451*, 232–240. https://dx.doi.org/10.1016/j.epsl.2016.06.040

Edmonds, H. N., German, C. R., Green, D. R. H., Huh, Y., Gamo, T., Edmond, J. M., 1996. Continuation of the hydrothermal fluid chemistry time series at TAG, and the effects of ODP drilling. *Geophys. Res. Lett. 23*(23), 3487–3489. https://dx.doi.org/10.1029/96gl01597

Eissen, J. P., Nohara, M., Cotten, J., Hirose, K., 1994. North Fiji Basin basalts and their magma sources: part I. incompatible element constraints. *Mar. Geol. 116*(1–2), 153–178. https://dx.doi.org/10.1016/0025-3227(94)90174-0

Elderfield, H., Schultz, A., 1996. Mid-ocean ridge hydrothermal fluxes and the chemical composition of the ocean. *Annu. Rev. Earth Planet. Sci. 24*, 191–224. https://dx.doi.org/10.1146/annurev.earth.24.1.191

Fernandez, A., Borrok, D. M., 2009. Fractionation of Cu, Fe, and Zn isotopes during the oxidative weathering of sulfide-rich rocks. *Chem. Geol. 264*(1–4), 1–12. https://dx.doi.org/10.1016/j.chemgeo.2009.01.024

Fouquet, Y., Pelleter, E., Konn, C., Chazot, G., Dupre, S., Ali, A.S., Chéron, S., Donval, J.P., Guyader, V., Etoubleau, J., Charlou, J.L., Labanieh, S., Scalabrin, C., 2018. Volcanic and hydrothermal processes in submarine calderas: The Kulo Lasi example (SW Pacific). *Ore Geol. Rev.* 99, 314–343.

Foustoukos, D. I., Seyfried, W. E., 2007. Quartz solubility in the two-phase and critical region of the NaCl–KCl–H_2O system: implications for submarine hydrothermal vent systems at 9°50′N East Pacific Rise. *Geochim. Cosmochim. Acta 71*(1), 186–201. https://dx.doi.org/10.1016/j.gca.2006.08.038

Francis, R. D., 1990. Sulfide globules in mid-ocean ridge basalts (MORB), and the effect of oxygen abundance in Fe-S-O liquids on the ability of those liquids to partition metals from MORB and komatiite magmas. *Chem. Geol.* 85, 199 – 213.

Frost, D. J., McCammon, C. A., 2008. The redox state of Earth's mantle. *Annu. Rev. Earth Planet. Sci. 36*, 389–420. https://dx.doi.org/10.1146/annurev.earth.36.031207.124322

Fujii, T., Moynier, F., Pons, M. L., Albarède, F., 2011. The origin of Zn isotope fractionation in sulfides. *Geochim. Cosmochim. Acta 75*(23), 7632–7643. https://dx.doi.org/10.1016/j.gca.2011.09.036

Gagnevin, D., Boyce, A. J., Barrie, C. D., Menuge, J. F., Blakeman, R. J., 2012. Zn, Fe and S isotope fractionation in a large hydrothermal system. *Geochim. Cosmochim. Acta 88*, 183–198. https://dx.doi.org/10.1016/j.gca.2012.04.031

Gallant, R. M., Von Damm, K. L., 2006. Geochemical controls on hydrothermal fluids from the Kairei and Edmond Vent Fields, 23°-25°S, Central Indian Ridge. *Geochem. Geophys. Geosyst. 7*(6), Q06018 https://dx.doi.org/10.1029/2005gc001067

German, C. R., Bennett, S. A., Connelly, D. P., Evans, A. J., Murton, B. J., Parson, L. M., Prien, R. D., Ramirez-Llodra, E. Z., Jakuba, M., Shank, T. M., Yoerger, D. R., Walker, S. L., Baker, E. T. and Nakamura, K., 2008. Hydrothermal activity on the southern Mid-Atlantic Ridge: tectonically- and volcanically-controlled venting at 4–5°S. *Earth Planet. Sci. Lett. 273*(3–4), 332–344. https://dx.doi.org/10.1016/j.epsl.2008.06.048

Grimaud, D., Ishibashi, J. I., Lagabrielle, Y., Auzende, J. M., Urabe, T., 1991. Chemistry of hydrothermal fluids from the 17°S active site on the North Fiji Basin Ridge (SW Pacific). *Chem. Geol. 93*(3–4), 209–218. https://dx.doi.org/10.1016/0009-2541(91)90114-7

Hannington, M.D., Herzig, P., Scott, S., Thompson, G., Rona, P., 1991. Comparative mineralogy and geochemistry of gold-bearing sulfide deposits on the mid-ocean ridges. *Mar. Geol.* 101, 217–248.

Heimann, A., Beard, B. L., Johnson, C. M., 2008. The role of volatile exsolution and sub-solidus fluid/rock interactions in producing high $^{56}Fe/^{54}Fe$ ratios in siliceous igneous rocks. *Geochim. Cosmochim. Acta 72*(17), 4379–4396. https://dx.doi.org/10.1016/j.gca.2008.06.009

Herzig, P. M., Hannington, M. D., 1995. Polymetallic massive sulfides at the modern seafloor a review. *Ore Geol. Rev.* 10, 95 - 115.

Herzog, G. F., Moynier, F., Albarède, F., Berezhnoy, A. A., 2009. Isotopic and elemental abundances of copper and zinc in lunar samples, Zagami, Pele's hairs, and a terrestrial basalt. *Geochim. Cosmochim. Acta 73*(19), 5884–5904. https://dx.doi.org/10.1016/j.gca.2009.05.067

Hibbert, K. E. J., Williams, H. M., Kerr, A. C., Puchtel, I. S., 2012. Iron isotopes in ancient and modern komatiites: evidence in support of an oxidised mantle from Archean to present. *Earth Planet. Sci. Lett. 321–322*, 198–207. https://dx.doi.org/10.1016/j.epsl.2012.01.011

Hofmann, A. W., 1997. Mantle geochemistry: the message from oceanic volcanism. *Nature*, *385*(6613), 219–229. https://dx.doi.org/10.1038/385219a0

Huang, J., Liu, S. A., Gao, Y., Xiao, Y., Chen, S., 2016. Copper and zinc isotope systematics of altered oceanic crust at IODP Site 1256 in the eastern equatorial Pacific. *J. Geophys. Res. Solid Earth 121*(10), 7086–7100. https://dx.doi.org/10.1002/2016jb013095

Ionov, D. A., Doucet, L. S., Ashchepkov, I. V., 2010. Composition of the lithospheric mantle in the Siberian craton: new constraints from fresh peridotites in the Udachnaya-East kimberlite. *J. Petrol. 51*(11), 2177–2210. https://dx.doi.org/10.1093/petrology/egq053

Ishibashi, J. I., Grimaud, D., Nojiri, Y., Auzende, J. M., Urabe, T., 1994a. Fluctuation of chemical compositions of the phase-separated hydrothermal fluid from the North Fiji Basin Ridge. *Mar. Geol. 116*(1–2), 215–226. https://dx.doi.org/10.1016/0025-3227(94)90177-5

Ishibashi, J. I., Wakita, H., Nojiri, Y., Grimaud, D., Jean-Baptiste, P., Gamo, T., Auzende, J. M., Urabe, T., 1994b. Helium and carbon geochemistry of hydrothermal fluids from the North Fiji Basin spreading ridge (southwest Pacific). *Earth Planet. Sci. Lett. 128*(3–4), 183–197. https://dx.doi.org/10.1016/0012-821x(94)90144-9

Ji, F., Zhou, H., Yang, Q., Gao, H., Wang, H., Lilley, M. D., 2017. Geochemistry of hydrothermal vent fluids and its implications for subsurface processes at the

active Longqi hydrothermal field, Southwest Indian Ridge. *Deep-Sea Res. I 122*, 41–47. https://dx.doi.org/10.1016/j.dsr.2017.02.001

John, S. G., Rouxel, O. J., Craddock, P. R., Engwall, A. M., Boyle, E. A., 2008. Zinc stable isotopes in seafloor hydrothermal vent fluids and chimneys. *Earth Planet. Sci. Lett. 269*(1–2), 17–28. https://dx.doi.org/10.1016/j.epsl.2007.12.011

Johnson, C. M., Skulan, J. L., Beard, B. L., Sun, H., Nealson, K. H., Braterman, P. S., 2002. Isotopic fractionation between Fe(III) and Fe(II) in aqueous solutions. *Earth Planet. Sci. Lett. 195*(1–2), 141–153. https://dx.doi.org/10.1016/s0012-821x(01)00581-7

Johnson, C. M., Beard, B. L., Beukes, N. J., Klein, C., O'Leary, J. M., 2003. Ancient geochemical cycling in the Earth as inferred from Fe isotope studies of banded iron formations from the Transvaal Craton. *Contrib. Mineral. Petrol. 144*(5), 523–547. https://dx.doi.org/10.1007/s00410-002-0418-x

Keith, M., Häckel, F., Haase, K. M., Schwarz-Schampera, U., Klemd, R., 2016. Trace element systematics of pyrite from submarine hydrothermal vents. *Ore Geol. Rev. 72*, 728–745. https://dx.doi.org/10.1016/j.oregeorev.2015.07.012

Kelley, K. D., Wilkinson, J. J., Chapman, J. B., Crowther, H. L., Weiss, D. J., 2009. Zinc isotopes in sphalerite from base metal deposits in the Red Dog district, northern Alaska. *Econ. Geol. 104*(6), 767–773. https://dx.doi.org/10.2113/gsecongeo.104.6.767

Kim, J., Lee, I., Halbach, P., Lee, K. Y., Ko, Y. T., Kim, K. H., 2006. Formation of hydrothermal vents in the North Fiji Basin: sulfur and lead isotope constraints. *Chem. Geol. 233*(3–4), 257–275. https://dx.doi.org/10.1016/j.chemgeo.2006.03.011

Kim, J., Moon, J. W., Lee, I., Kim, Y., Larson, P., 2014. *Copper isotope composition of seafloor hydrothermal vents in back-arc and arc settings, western Pacific*. Paper presented at Goldschmidt Conference 2014, Geochemical Society and European Association of Geochemistry, Sacramento, CA.

Klein, E. M., Langmuir, C. H., 1987. Global correlations of ocean ridge basalt chemistry with axial depth and crustal thickness. *J. Geophys. Res. Solid Earth 92*(B8), 8089–8115. https://dx.doi.org/10.1029/jb092ib08p08089

Koschinsky, A., Seifert, R., Halbach, P., Bau, M., Brasse, S., de Carvalho, L. M., Fonseca, N. M., 2002. Geochemistry of diffuse low-temperature hydrothermal fluids in the North Fiji basin. *Geochim. Cosmochim. Acta 66*(8), 1409–1427. https://dx.doi.org/10.1016/s0016-7037(01)00855-9

Kumagai, H., Nakamura, K., Toki, T., Morishita, T., Okino, K., Ishibashi, J. -I., Tsunogai, U., Kawagucci, S., Gamo, T., Shibuya, T., Sawaguchi, T., Neo, N., Joshima, M., Sato, T., Takai, K., 2008. Geological background of the Kairei and Edmond hydrothermal fields along the Central Indian Ridge: Implications of their

vent fluids' distinct chemistry. *Geofluids*, *8*(4), 239–251. https://dx.doi.org/10.1111/j.1468-8123.2008.00223.x

Kunzmann, M., Halverson, G. P., Sossi, P. A., Raub, T. D., Payne, J. L., Kirby, J., 2013. Zn isotope evidence for immediate resumption of primary productivity after snowball Earth. *Geology*, *41*(1), 27–30. https://dx.doi.org/10.1130/g33422.1

Le Roux, V., Dasgupta, R., Lee, C. T. A., 2011. Mineralogical heterogeneities in the Earth's mantle: constraints from Mn, Co, Ni and Zn partitioning during partial melting. *Earth Planet. Sci. Lett. 307*(3–4), 395–408. https://dx.doi.org/10.1016/j.epsl.2011.05.014

Li, W., Jackson, S. E., Pearson, N. J., Alard, O., Chappell, B. W., 2009. The Cu isotopic signature of granites from the Lachlan Fold Belt, SE Australia. *Chem. Geol. 258*(1–2), 38–49. https://dx.doi.org/10.1016/j.chemgeo.2008.06.047

Little, S. H., Vance, D., Walker-Brown, C., Landing, W. M., 2014. The oceanic mass balance of copper and zinc isotopes, investigated by analysis of their inputs, and outputs to ferromanganese oxide sediments. *Geochim. Cosmochim. Acta 125*, 673–693. https://dx.doi.org/10.1016/j.gca.2013.07.046

Liu, S. -A., Huang, J., Liu, J., Wörner, G., Yang, W., Tang, Y. -J., Chen, Y., Tang, L. -M., Zheng, J. -P., Li, S. -G., 2015. Copper isotopic composition of the silicate Earth. *Earth Planet. Sci. Lett. 427*, 95–103. https://dx.doi.org/10.1016/j.epsl.2015.06.061

Liu, S. A., Wang, Z. Z., Li, S. G., Huang, J., Yang, W., 2016. Zinc isotope evidence for a large-scale carbonated mantle beneath eastern China. *Earth Planet. Sci. Lett. 444*, 169–178. https://dx.doi.org/10.1016/j.epsl.2016.03.051

Lodders, K., 2003. Solar system abundances and condensation temperatures of the elements. *Astrophys. J. 591*(2), 1220–1247. https://dx.doi.org/10.1086/375492

Maréchal, C. N., Télouk, P., Albarède, F., 1999. Precise analysis of copper and zinc isotopic compositions by plasma-source mass spectrometry. *Chem. Geol. 156*(1–4), 251–273. https://dx.doi.org/10.1016/s0009-2541(98)00191-0

Maréchal, C. N., Sheppard, S. M. F., 2002. Isotopic fractionation of Cu and Zn between chloride and nitrate solutions and malachite or smithsonite at 30° and 50°C. *Geochim. Cosmochim. Acta 66*(S1), A84. https://dx.doi.org/10.1016/S0016-7037(02)01007-4

Markl, G., Lahaye, Y., Schwinn, G., 2006. Copper isotopes as monitors of redox processes in hydrothermal mineralization. *Geochim. Cosmochim. Acta 70*(16), 4215–4228. https://dx.doi.org/10.1016/j.gca.2006.06.1369

Mason, T. F. D., Weiss, D. J., Chapman, J. B., Wilkinson, J. J., Tessalina, S. G., Spiro, B., Horstwood, M. S., Spratt, J., Coles, B. J., 2005. Zn and Cu isotopic variability in the Alexandrinka volcanic-hosted massive sulphide (VHMS) ore deposit, Urals, Russia. *Chem. Geol. 221*(3–4), 170–187. https://dx.doi.org/10.1016/j.chemgeo.2005.04.011

Merlivat, L., Pineau, F., Javoy, M., 1987. Hydrothermal vent waters at 13°N on the East Pacific Rise: isotopic composition and gas concentration. *Earth Planet. Sci. Lett.* *84*(1), 100–108. https://dx.doi.org/10.1016/0012-821x(87)90180-4

Michard, G., Albarède, F., Michard, A., Minster, J. F., Charlou, J. L., Tan, N., 1984. Chemistry of solutions from the 13°N East Pacific Rise hydrothermal site. *Earth Planet. Sci. Lett. 67*(3), 297–307. https://dx.doi.org/10.1016/0012-821x(84)90169-9

Moeller, K., Schoenberg, R., Pedersen, R. B., Weiss, D., Dong, S., 2012. Calibration of the new certified reference materials ERM-AE633 and ERM-AE647 for copper and IRMM-3702 for zinc isotope amount ratio determinations. *Geostand. Geoanal. Res. 36*(2), 177–199. https://dx.doi.org/10.1111/j.1751-908x.2011.00153.x

Moeller, K., Schoenberg, R., Grenne, T., Thorseth, I. H., Drost, K., Pedersen, R. B., 2014. Comparison of iron isotope variations in modern and Ordovician siliceous Fe oxyhydroxide deposits. *Geochim. Cosmochim. Acta 126*, 422–440. https://dx.doi.org/10.1016/j.gca.2013.11.018

Nohara, M., Hirose, K., Eissen, J. P., Urabe, T., Joshima, M., 1994. The North Fiji Basin basalts and their magma sources: part II. Sr-Nd isotopic and trace element constraints. *Mar. Geol. 116*(1–2), 179–195. https://dx.doi.org/10.1016/0025-3227(94)90175-9

O´Neill, H. St.C., Berry, A. J., Mallmann, G., 2018. The oxidation state of iron in Mid-Ocean Ridge Basaltic (MORB) glasses: Implications for their petrogenesis and oxygen fugacities. *Earth Planet. Sci. Lett.* 504, 152 – 162.

Oosting, S. E., Von Damm, K. L., 1996. Bromide/chloride fractionation in seafloor hydrothermal fluids from 9–10°N East Pacific Rise. *Earth Planet. Sci. Lett.* *144*(1–2), 133–145. https://dx.doi.org/10.1016/0012-821x(96)00149-5

Patriat, P., Segoufin, J., 1988. Reconstruction of the Central Indian Ocean. *Tectonophysics*, *155*(1–4), 211–234. https://dx.doi.org/10.1016/0040-1951(88)90267-3

Pękala, M., Asael, D., Butler, I. B., Matthews, A., Rickard, D., 2011. Experimental study of Cu isotope fractionation during the reaction of aqueous Cu(II) with Fe(II) sulphides at temperatures between 40 and 200°C. *Chem. Geol. 289*(1–2), 31–38. https://dx.doi.org/10.1016/j.chemgeo.2011.07.004

Petit, J. C. J., de Jong, J., Chou, L., Mattielli, N., 2008. Development of Cu and Zn isotope MC-ICP-MS measurements: application to suspended particulate matter and sediments from the Scheldt estuary. *Geostand. Geoanal. Res. 32*(2), 149–166. https://dx.doi.org/10.1111/j.1751-908x.2008.00867.x

Pichat, S., Douchet, C., Albarède, F., 2003. Zinc isotope variations in deep-sea carbonates from the eastern equatorial Pacific over the last 175 ka. *Earth Planet. Sci. Lett. 210*(1–2), 167–178. https://dx.doi.org/10.1016/s0012-821x(03)00106-7

Poitrasson, F., Freydier, R., 2005. Heavy iron isotope composition of granites determined by high resolution MC-ICP-MS. *Chem. Geol. 222*(1–2), 132–147. https://dx.doi.org/10.1016/j.chemgeo.2005.07.005

Polyakov, V. B., Mineev, S. D., 2000. The use of Mössbauer spectroscopy in stable isotope geochemistry. *Geochim. Cosmochim. Acta 64*(5), 849–865. https://dx.doi.org/10.1016/s0016-7037(99)00329-4

Polyakov, V. B., Soultanov, D., 2010. *Iron isotope fractionation in sulfide: constraints on mechanisms of sulfide formations in hydrothermal and magmatic systems*. Paper presented at EGU General Assembly 2010, European Geosciences Union, Vienna, Austria.

Ponzevera, E., Quétel, C. R., Berglund, M., Taylor, P. D. P., Evans, P., Loss, R. D., Fortunato, G., 2006. Mass discrimination during MC-ICPMS isotopic ratio measurements: investigation by means of synthetic isotopic mixtures (IRMM-007 series) and application to the calibration of natural-like zinc materials (including IRMM-3702 and IRMM-651). *J. Am. Soc. Mass Spectrom. 17*(10), 1413–1427. https://dx.doi.org/10.1016/j.jasms.2006.06.001

Proskurowski, G., Lilley, M. D., Olson, E. J., 2008. Stable isotopic evidence in support of active microbial methane cycling in low-temperature diffuse flow vents at 9°50′N East Pacific Rise. *Geochim. Cosmochim. Acta 72*(8), 2005–2023. https://dx.doi.org/10.1016/j.gca.2008.01.025

Prytulak, J., Elliott, T., 2007. TiO_2 enrichment in ocean island basalts. *Earth Planet. Sci. Lett. 263*(3–4), 388–403. https://dx.doi.org/10.1016/j.epsl.2007.09.015

Reisberg, L., Zhi, X., Lorand, J. P., Wagner, C., Peng, Z., Zimmermann, C., 2005. Re–Os and S systematics of spinel peridotite xenoliths from east central China: evidence for contrasting effects of melt percolation. *Earth Planet. Sci. Lett. 239*(3–4), 286–308. https://dx.doi.org/10.1016/j.epsl.2005.09.010

Rouxel, O., Dobbek, N., Ludden, J., Fouquet, Y., 2003. Iron isotope fractionation during oceanic crust alteration. *Chem. Geol. 202*(1–2), 155–182. https://dx.doi.org/10.1016/j.chemgeo.2003.08.011

Rouxel, O., Fouquet, Y., Ludden, J. N., 2004a. Copper isotope systematics of the Lucky Strike, Rainbow, and Logatchev sea-floor hydrothermal fields on the Mid-Atlantic Ridge. *Econ. Geol. 99*(3), 585–600. https://dx.doi.org/10.2113/gsecongeo.99.3.585

Rouxel, O., Fouquet, Y., Ludden, J. N., 2004b. Subsurface processes at the lucky strike hydrothermal field, Mid-Atlantic ridge: evidence from sulfur, selenium, and iron isotopes. *Geochim. Cosmochim. Acta 68*(10), 2295–2311. https://dx.doi.org/10.1016/j.gca.2003.11.029

Rouxel, O., Shanksiii, W., Bach, W., Edwards, K. J., 2008. Integrated Fe- and S-isotope study of seafloor hydrothermal vents at East Pacific Rise 9–10°N. *Chem. Geol. 252*(3–4), 214–227. https://dx.doi.org/10.1016/j.chemgeo.2008.03.009

Rouxel, O., Auro, M., 2010. Iron isotope variations in coastal seawater determined by multicollector ICP-MS. *Geostand. Geoanal. Res. 34*(2), 135–144. https://dx.doi.org/10.1111/j.1751-908x.2010.00063.x

Salters, V. J. M., Mallick, S., Hart, S. R., Langmuir, C. E., Stracke, A., 2011. Domains of depleted mantle: new evidence from hafnium and neodymium isotopes. *Geochem. Geophys. Geosyst. 12*(8), Q08001. https://dx.doi.org/10.1029/2011gc003617

Samanta, M., Ellwood, M. J., Sinoir, M., Hassler, C. S., 2017. Dissolved zinc isotope cycling in the Tasman Sea, SW Pacific Ocean. *Mar. Chem. 192*, 1–12. https://dx.doi.org/10.1016/j.marchem.2017.03.004

Savage, P. S., Harvey, J., Moynier, F., 2014. *Copper isotope heterogeneity in the lithospheric mantle*. Paper presented at Goldschmidt Conference 2014, Geochemical Society and European Association of Geochemistry, Sacramento, CA.

Savage, P. S., Moynier, F., Chen, H., Shofner, G., Siebert, J., Badro, J., Puchtel, I. S., 2015. Copper isotope evidence for large-scale sulphide fractionation during Earth's differentiation. *Geochem. Perspect. Lett. 1*(1), 53–64. https://dx.doi.org/10.7185/geochemlet.1506

Schauble, E. A., Rossman, G. R., Taylor, H. P., 2001. Theoretical estimates of equilibrium Fe-isotope fractionations from vibrational spectroscopy. *Geochim.*

Cosmochim. Acta 65(15), 2487–2497.

https://dx.doi.org/10.1016/s0016-7037(01)00600-7

Schmidt, K., Koschinsky, A., Garbe-Schönberg, D., de Carvalho, L. M., Seifert, R., 2007. Geochemistry of hydrothermal fluids from the ultramafic-hosted Logatchev hydrothermal field, 15°N on the Mid-Atlantic Ridge: temporal and spatial investigation. *Chem. Geol. 242*(1–2), 1–21.

https://dx.doi.org/10.1016/j.chemgeo.2007.01.023

Schoenberg, R., von Blanckenburg, F., 2006. Modelling of planetary-scale Fe isotope fractionation. *Earth Planet. Sci. Lett. 252*(3–4), 342–359.

https://dx.doi.org/10.1016/j.epsl.2006.09.045

Schuessler, J. A., Schoenberg, R., Sigmarsson, O., 2009. Iron and lithium isotope systematics of the Hekla volcano, Iceland—evidence for Fe isotope fractionation during magma differentiation. *Chem. Geol. 258*(1–2), 78–91.

https://dx.doi.org/10.1016/j.chemgeo.2008.06.021

Searle, R. C., 1983. Multiple, closely spaced transform faults in fast-slipping fracture zones. *Geology*, *11*(10), 607–610.

https://dx.doi.org/10.1130/0091-7613(1983)11<607:mcstfi>2.0.co;2

Severmann, S., Johnson, C. M., Beard, B. L., German, C. R., Edmonds, H. N., Chiba, H., Green, D. R. H., 2004. The effect of plume processes on the Fe isotope composition of hydrothermally derived Fe in the deep ocean as inferred from the

Rainbow vent site, Mid-Atlantic Ridge, 36°14′N. *Earth Planet. Sci. Lett.* *225*(1–2), 63–76. https://dx.doi.org/10.1016/j.epsl.2004.06.001

Sharma, M., Polizzotto, M., Anbar, A. D., 2001. Iron isotopes in hot springs along the Juan de Fuca Ridge. *Earth Planet. Sci. Lett. 194*(1–2), 39–51. https://dx.doi.org/10.1016/s0012-821x(01)00538-6

Shields, W. R., Goldich, S. S., Garner, E. L., Murphy, T. J., 1965. Natural variations in the abundance ratio and the atomic weight of copper. *J. Geophys. Res. 70*(2), 479–491. https://dx.doi.org/10.1029/jz070i002p00479

Sossi, P. A., Halverson, G. P., Nebel, O., Eggins, S. M., 2015. Combined separation of Cu, Fe and Zn from rock matrices and improved analytical protocols for stable isotope determination. *Geostand. Geoanal. Res. 39*(2), 129–149. https://dx.doi.org/10.1111/j.1751-908x.2014.00298.x

Stracke, A., Hofmann, A. W., Hart, S. R., 2005. FOZO, HIMU, and the rest of the mantle zoo. *Geochem. Geophys. Geosyst. 6*(5), Q05007. https://dx.doi.org/10.1029/2004gc000824

Sun, S. McDonough, W. F., 1989. Chemical and isotopic systematics of oceanic basalts; implications for mantle composition and processes. *Geological Society, London, Special Publications*, 42 (1), 313–345.

Taylor, P. D. P., Maeck, R., De Bièvre, P., 1992. Determination of the absolute isotopic composition and Atomic Weight of a reference sample of natural iron. *Int. J. Mass*

Spectrom. Ion Proc. 121(1–2), 111–125. https://dx.doi.org/10.1016/0168-1176(92)80075-c

Telus, M., Dauphas, N., Moynier, F., Tissot, F. L. H., Teng, F. Z., Nabelek, P. I., Craddock, P. R., Groat, L. A., 2012. Iron, zinc, magnesium and uranium isotopic fractionation during continental crust differentiation: the tale from migmatites, granitoids, and pegmatites. *Geochim. Cosmochim. Acta 97*, 247–265. https://dx.doi.org/10.1016/j.gca.2012.08.024

Teng, F. Z., Dauphas, N., Helz, R. T., 2008. Iron isotope fractionation during magmatic differentiation in Kilauea Iki lava lake. *Science*, *320*(5883), 1620–1622. https://dx.doi.org/10.1126/science.1157166

Teng, F. Z., Dauphas, N., Helz, R. T., Gao, S., Huang, S., 2011. Diffusion-driven magnesium and iron isotope fractionation in Hawaiian olivine. *Earth Planet. Sci. Lett. 308*(3–4), 317–324. https://dx.doi.org/10.1016/j.epsl.2011.06.003

Teng, F. Z., Dauphas, N., Huang, S., Marty, B., 2013. Iron isotopic systematics of oceanic basalts. *Geochim. Cosmochim. Acta 107*, 12–26. https://dx.doi.org/10.1016/j.gca.2012.12.027

Toutain, J. P., Sonke, J., Munoz, M., Nonell, A., Polvé, M., Viers, J., Freydier, R., Sortino, F., Joron, J. L., Sumarti, S., 2008. Evidence for Zn isotopic fractionation at Merapi volcano. *Chem. Geol. 253*(1–2), 74–82. https://dx.doi.org/10.1016/j.chemgeo.2008.04.007

Urey, H. C., 1947. The thermodynamic properties of isotopic substances. *J. Chem. Soc. 1947*, 562–581. https://dx.doi.org/10.1039/jr9470000562

Vance, D., Archer, C., Bermin, J., Perkins, J., Statham, P. J., Lohan, M. C., Ellwood, M. J., Mills, R. A., 2008. The copper isotope geochemistry of rivers and the oceans. *Earth Planet. Sci. Lett. 274*(1–2), 204–213. https://dx.doi.org/10.1016/j.epsl.2008.07.026

Van Dover, C. L., Humphris, S. E., Fornari, D., Cavanaugh, C. M., Collier, R., Goffredi, S. K., Hashimoto, J., Lilley, M. D., Reysenbach, A. L., Shank, T. M., Von Damm, K. L., Banta, A., Gallant, R. M., Götz, D., Green, D., Hall, J., Harmer, T. L., Hurtado, L. A., Johnson, P., McKiness, Z. P., Meredith, C., Olson, E., Pan, I. L., Turnipseed, M., Won, Y., Young III, C. R., Vrijenhoek, R. C., 2001. Biogeography and ecological setting of Indian Ocean hydrothermal vents. *Science*, *294*(5543), 818–823. https://dx.doi.org/10.1126/science.1064574

Wang, Z. -Z., Liu, S. -A., Liu, J., Huang, J., Xiao, Y., Chu, Z. -Y., Zhao, X. -M., Tang, L., 2017. Zinc isotope fractionation during mantle melting and constraints on the Zn isotope composition of Earth's upper mantle. *Geochim. Cosmochim. Acta 198*, 151–167. https://dx.doi.org/10.1016/j.gca.2016.11.014

Weyer, S., Anbar, A. D., Brey, G. P., Münker, C., Mezger, K., Woodland, A. B., 2005. Iron isotope fractionation during planetary differentiation. *Earth Planet. Sci. Lett. 240*(2), 251–264. https://dx.doi.org/10.1016/j.epsl.2005.09.023

Weyer, S., Ionov, D. A., 2007. Partial melting and melt percolation in the mantle: the message from Fe isotopes. *Earth Planet. Sci. Lett. 259*(1–2), 119–133. https://dx.doi.org/10.1016/j.epsl.2007.04.033

Weyer, S., Seitz, H. M., 2012. Coupled lithium- and iron isotope fractionation during magmatic differentiation. *Chem. Geol. 294–295*, 42–50. https://dx.doi.org/10.1016/j.chemgeo.2011.11.020

Wilkinson, J. J., Weiss, D. J., Mason, T. F. D., Coles, B. J., 2005. Zinc isotope variation in hydrothermal systems: preliminary evidence from the Irish Midlands ore field. *Econ. Geol. 100*(3), 583–590. https://doi.org/10.2113/gsecongeo.100.3.583

Williams, H. M., Nielsen, S. G., Renac, C., Griffin, W. L., O'Reilly, S. Y., McCammon, C. A., Pearson, N., Viljoen, F., Alt, J. C., Halliday, A. N., 2009. Fractionation of oxygen and iron isotopes by partial melting processes: implications for the interpretation of stable isotope signatures in mafic rocks. *Earth Planet. Sci. Lett. 283*(1–4), 156–166. https://dx.doi.org/10.1016/j.epsl.2009.04.011

Williams, H. M., Bizimis, M., 2014. Iron isotope tracing of mantle heterogeneity within the source regions of oceanic basalts. *Earth Planet. Sci. Lett. 404*, 396–407. https://dx.doi.org/10.1016/j.epsl.2014.07.033

Woodhead, J. D., Johnson, R. W., 1993. Isotopic and trace-element profiles across the New Britain island arc, Papua New Guinea. *Contrib. Mineral. Petrol. 113*(4), 479–491. https://dx.doi.org/10.1007/bf00698317

Woodhead, J. D., Eggins, S. M., Johnson, R. W., 1998. Magma genesis in the New Britain island arc: further insights into melting and mass transfer processes. *J. Petrol. 39*(9), 1641–1668. https://dx.doi.org/10.1093/petroj/39.9.1641

Workman, R. K., Hart, S. R., Jackson, M., Regelous, M., Farley, K. A., Blusztajn, J., Kurz, M., Staudigel, H., 2004. Recycled metasomatized lithosphere as the origin of the Enriched Mantle II (EM2) end-member: evidence from the Samoan volcanic chain. *Geochem. Geophys. Geosyst. 5*(4), Q04008. https://dx.doi.org/10.1029/2003gc000623

Workman, R. K., Hart, S. R., 2005. Major and trace element composition of the depleted MORB mantle (DMM). *Earth Planet. Sci. Lett. 231*(1–2), 53–72. https://dx.doi.org/10.1016/j.epsl.2004.12.005

Wu, J., Boyle, E. A., 1997. Low blank preconcentration technique for the determination of lead, copper, and cadmium in small-volume seawater samples by isotope dilution ICPMS. *Anal. Chem. 69*(13), 2464–2470. https://dx.doi.org/10.1021/ac961204u

Yamaoka, K., Hong, E., Ishikawa, T., Gamo, T., Kawahata, H., 2015. Boron isotope geochemistry of vent fluids from arc/back-arc seafloor hydrothermal systems in the western Pacific. *Chem. Geol. 392*, 9–18. https://dx.doi.org/10.1016/j.chemgeo.2014.11.009

Zeng, Z., Chen, D., Yin, X., Wang, X., Zhang, G., Wang, X., 2010. Elemental and isotopic compositions of the hydrothermal sulfide on the East Pacific Rise near 13°N. *Sci. China Earth Sci. 53*(2), 253–266. https://dx.doi.org/10.1007/s11430-010-0013-3

Zeng, Z., Chen, S., Selby, D., Yin, X., Wang, X., 2014. Rhenium–osmium abundance and isotopic compositions of massive sulfides from modern deep-sea hydrothermal systems: implications for vent associated ore forming processes. *Earth Planet. Sci. Lett. 396*, 223–234. https://dx.doi.org/10.1016/j.epsl.2014.04.017

Zeng, Z., Ma, Y., Yin, X., Selby, D., Kong, F., Chen, S., 2015a. Factors affecting the rare earth element compositions in massive sulfides from deep-sea hydrothermal systems. *Geochem. Geophys. Geosyst. 16*(8), 2679–2693. https://dx.doi.org/10.1002/2015gc005812

Zeng, Z., Niedermann, S., Chen, S., Wang, X., Li, Z., 2015b. Noble gases in sulfide deposits of modern deep-sea hydrothermal systems: implications for heat fluxes and hydrothermal fluid processes. *Chem. Geol. 409*, 1–11. https://dx.doi.org/10.1016/j.chemgeo.2015.05.007

Zeng, Z., Ma, Y., Chen, S., Selby, D., Wang, X., Yin, X., 2017. Sulfur and lead isotopic compositions of massive sulfides from deep-sea hydrothermal systems:

implications for ore genesis and fluid circulation. *Ore Geol. Rev. 87*, 155–171. https://dx.doi.org/10.1016/j.oregeorev.2016.10.014

Zhao, X., Zhang, H., Zhu, X., Tang, S., Yan, B., 2012. Iron isotope evidence for multistage melt–peridotite interactions in the lithospheric mantle of eastern China. *Chem. Geol. 292–293*, 127–139. https://dx.doi.org/10.1016/j.chemgeo.2011.11.016

Zhao, X., Zhang, H., Zhu, X., Zhu, B., Cao, H., 2015. Effects of melt percolation on iron isotopic variation in peridotites from Yangyuan, North China Craton. *Chem. Geol. 401*, 96–110. https://dx.doi.org/10.1016/j.chemgeo.2015.02.031

Zhao, Y., Vance, D., Abouchami, W., de Baar, H. J. W., 2014. Biogeochemical cycling of zinc and its isotopes in the Southern Ocean. *Geochim. Cosmochim. Acta 125*, 653–672. https://dx.doi.org/10.1016/j.gca.2013.07.045

Zheng, J. P., Zhang, R. Y., Griffin, W. L., Liou, J. G., O'Reilly, S. Y., 2005. Heterogeneous and metasomatized mantle recorded by trace elements in minerals of the Donghai garnet peridotites, Sulu UHP terrane, China. *Chem. Geol. 221*(3–4), 243–259. https://dx.doi.org/10.1016/j.chemgeo.2005.05.002

Zhou, J. X., Huang, Z. L., Zhou, M. F., Zhu, X. K., Muchez, P., 2014. Zinc, sulfur and lead isotopic variations in carbonate-hosted Pb–Zn sulfide deposits, southwest China. *Ore Geol. Rev. 58*, 41–54. https://dx.doi.org/10.1016/j.oregeorev.2013.10.009

Zhu, X. K., O'Nions, R. K., Guo, Y., Belshaw, N. S., Rickard, D., 2000. Determination of natural Cu-isotope variation by plasma-source mass spectrometry: implications for use as geochemical tracers. *Chem. Geol. 163*(1–4), 139–149. https://dx.doi.org/10.1016/s0009-2541(99)00076-5

Fig. 1. Locations of the seafloor mid-ocean ridge sulfide (MORS), back-arc basin sulfide (BABS), and their host mid-ocean ridge basalt (MORB) samples from deep-sea hydrothermal fields analyzed for Fe, Cu, and Zn isotope compositions. EHF: Edmond hydrothermal field; CIR: Central Indian Ridge; SWIR: Southwest Indian Ridge; S99HF: Sonne 99 hydrothermal field; NFB: North Fiji back-arc basin; EPR: East Pacific Rise.

Fig. 2. (a) Trace element patterns normalized to primitive mantle concentrations, and (b) REE patterns normalized to chondritic values for the EPR13°N, EPR 1−2°S, CIR, and SWIR volcanic rocks. The primitive mantle and chondrite normalization values are from Sun and McDonough (1989).

Fig. 3. δ^{56}Fe values of the mid-ocean ridge basalt (MORB), mid-ocean ridge sulfide

(MORS), and back-arc basin sulfides (BABS) samples. The δ^{56}Fe ranges of previously studied MORBs (Teng et al., 2013), ocean island basalts (OIBs) (Beard et al., 2003; Teng et al., 2013), seawater (Rouxel & Auro, 2010), sediments (Rouxel et al., 2003; Severmann et al., 2004), and hydrothermal fluids (Moeller et al., 2014; Rouxel et al., 2008; Severmann et al., 2004; Sharma et al., 2001), basalts from the North Fiji back-arc basin (Teng et al., 2013), and MORS minerals from the EPR between 9° and 10°N (Rouxel et al., 2008) and the JdFR (Sharma et al., 2001) are also illustrated. Py: pyrite; Cpy: chalcopyrite; Sp: sphalerite.

Fig. 4. δ^{65}Cu values of the mid-ocean ridge basalt (MORB), mid-ocean ridge sulfide (MORS), and back-arc basin sulfides (BABS) samples. The δ^{65}Cu value ranges of previously studied MORBs (Liu et al., 2015; Savage et al., 2015), ocean island basalts (OIBs) (Liu et al., 2015; Savage et al., 2015), seawater (Little et al., 2014; Vance et al., 2008), sediments (Maréchal et al., 1999), and hydrothermal fluids (Dekov & Rouxel, 2012) are also presented.

Fig. 5. δ^{66}Zn values of the mid-ocean ridge basalt (MORB), mid-ocean ridge sulfide (MORS), and back-arc basin sulfides (BABS) samples. The δ^{66}Zn value ranges of

previously studied MORBs (Ben Othman et al., 2006; Wang et al., 2017), ocean island basalts (OIBs) (Wang et al., 2017), seawater (Little et al., 2014; Samanta et al., 2017; Y. Zhao et al., 2014), sediments (Maréchal et al., 1999; Pichat et al., 2003), and hydrothermal fluids (John et al., 2008) are also shown.

Fig. 6. Plots of mid-ocean ridge (MOR) spreading rate vs. (a) δ^{56}Fe, (b) δ^{65}Cu, and (c) δ^{66}Zn for the mid-ocean ridge basalts (MORBs) reported in this study.

Fig. 7. Plots of hydrothermal fluid temperature vs. (a) δ^{56}Fe of sulfides, (b) δ^{65}Cu of chalcopyrite, and (c) δ^{66}Zn of sphalerite from seafloor hydrothermal fields. The temperature data for the hydrothermal fluids are from Bowers et al. (1988), Grimaud et al. (1991), Ishibashi et al. (1994a, b), Oosting and Von Damm (1996), Gallant and Von Damm (2006), Foustoukos and Seyfried (2007), John et al. (2008), Proskurowski et al. (2008), Rouxel et al. (2008), Ji et al. (2017), and Yamaoka et al. (2015).

Table 1 Fe-Cu-Zn isotopic compositions of the mid-ocean ridge basalts (MORBs) and reference materials.

Sample Name	Ty	Locatio	δ^{56}	2S	δ^{57}	2S	N	δ^{65}	2S	N	δ^{68}	2S	δ^{66}	2S	N
E27-1	bas	EPR13º	0.1	0.	0.1	0.	6	0.2	0.	3	0.6	0.	0.3	0.	3
E29-1	bas	EPR13º	0.1	0.	0.1	0.	3	0.2	0.	3	0.7	0.	0.3	0.	3
E33-1	bas	EPR13º	0.1	0.	0.1	0.	4	0.0	0.	3	0.6	0.	0.3	0.	3

E44-1	bas	EPR13º	0.1	0.	0.2	0.	3	0.0	0.	3	0.7	0.	0.3	0.	3
E44-1*	bas	EPR13º	0.1	0.	0.1	0.	4	0.4	0.	3	0.6	0.	0.3	0.	3
E46	bas	EPR13º	0.1	0.	0.1	0.	3	0.3	0.	3	0.6	0.	0.3	0.	3
EPR05-TVG4	bas	EPR1-2	0.1	0.	0.1	0.	3	0.2	0.	3	0.6	0.	0.3	0.	3
20III-S4-TVG1	bas	EPR1-2	0.1	0.	0.1	0.	3	0.3	0.	3	0.6	0.	0.3	0.	3
20III-S8-TVG5-1	bas	EPR1-2	0.1	0.	0.1	0.	4	0.5	0.	3	0.6	0.	0.3	0.	3
20III-S10-TVG7	bas	EPR1-2	0.1	0.	0.2	0.	3	0.5	0.	3	0.8	0.	0.4	0.	6
20III-S10-TVG7*	bas	EPR1-2	0.1	0.	0.2	0.	3	0.1	0.	3	0.9	0.	0.4	0.	3
20III-S11-TVG8-1	bas	EPR1-2	0.1	0.	0.2	0.	3	0.0	0.	3	0.7	0.	0.3	0.	3
21III-S18-TVG14	bas	EPR1-2	0.0	0.	0.1	0.	5	0.5	0.	3	0.7	0.	0.3	0.	3
IR05-TVG10-1	bas	EHF,	0.1	0.	0.1	0.	4	-0.	0.	3	0.8	0.	0.4	0.	3
IR05-TVG11-1	bas	EHF,	0.1	0.	0.1	0.	5	0.1	0.	3	0.8	0.	0.4	0.	2
IR05-TVG1-1	bas	A area,	0.1	0.	0.1	0.	6	0.3	0.	3	0.8	0.	0.4	0.	3
IR05-TVG3-1	bas	A area,	0.1	0.	0.2	0.	4	-0.	0.	3	0.9	0.	0.4	0.	3
IR05-TVG4-1	bas	A area,	0.1	0.	0.2	0.	4	0.6	0.	3	0.9	0.	0.4	0.	3
IR05-TVG4-1*	bas	A area,	0.1	0.	0.2	0.	6	0.7	0.	1	0.9	0.	0.4	0.	5
IR05-TVG5-1	bas	A area,	0.1	0.	0.2	0.	5	0.3	0.	3	0.9	0.	0.4	0.	3
20IV-S4-TVG1	bas	A area,	0.1	0.	0.1	0.	3	0.5	0.	3	0.8	0.	0.4	0.	3
20V-S11-TVG3	bas	A area,	0.0	0.	0.1	0.	3	0.4	0.	3	0.8	0.	0.4	0.	3
20V-S34-TVG16	bas	A area,	0.0	0.	0.1	0.	5	0.4	0.	3	0.9	0.	0.4	0.	3
20VII-S3-TVG3	bas	A area,	0.1	0.	0.1	0.	3	0.2	0.	3	1.0	0.	0.5	0.	3
20VII-S7-TVG5	bas	A area,	0.1	0.	0.2	0.	3	0.0	0.	3	1.0	0.	0.5	0.	2
20VII-S7-TVG5*	bas	A area,	0.1	0.	0.1	0.	3	0.0	0.	3	1.0	0.	0.4	0.	2
20VII-S15-TVG13-1	bas	A area,	0.1	0.	0.2	0.	3	0.1	0.	3	1.0	0.	0.4	0.	3
20VII-S20-TVG17-1	bas	A area,	0.1	0.	0.2	0.	3	-0.	0.	3	0.9	0.	0.4	0.	2
Reference materials															
IRMM-014			0.0	0.	0.0	0.	4								
MIX			-2.	0.	-2.	0.	2								
Average Quality control			-2.	0.	-2.	0.	6								
JMC Cu110 in-house								1.0	0.	3					
SRM NIST 976 Cu								-0.	0.	2					
BHVO-2								0.0	0.	9					
JMC Zn310 in-house											-0.	0.	-0.	0.	2
IRMM-3702 Zn											0.6	0.	0.3	0.	8

* Indicates the analysis result of a duplicate sample.

Table 2 Fe-Cu-Zn isotopic compositions of seafloor hydrothermal sulfides from mid-ocean ridge basalts (MORBs), back-arc basin basalt (BABBs), and reference materials.

Sample Name	Miner	Location	δ^{56}Fe	2SD	δ^{57}Fe	2SD	N	δ^{65}Cu	2SD	N	δ^{68}Z	2SD	δ^{66}Z	2SD	N
Mid-ocean ridge sulfides (MORS)															
EPR05-TVG1-2-1	Py	EPR13ºN	-0.31	0.09	-0.41	0.09	6								
EPR05-TVG1-2-1*	Py	EPR13ºN	-0.29	0.05	-0.40	0.16	6								
EPR05-TVG1-2-4	Py	EPR13ºN	-0.38	0.10	-0.57	0.20	6								
EPR05-TVG1-3-2	Py	EPR13ºN	-0.86	0.08	-1.30	0.16	5								
EPR05-TVG1-3-3	Py	EPR13ºN	-0.83	0.06	-1.26	0.07	3								
EPR05-TVG2-1-2	Py	EPR13ºN	-1.05	0.08	-1.58	0.21	3								
EPR05-TVG2-1-4	Py	EPR13ºN	-0.88	0.10	-1.34	0.13	5								
20III-S4-TVG1-1-1	Py	EPR1-2ºS	-0.75	0.06	-1.11	0.14	3								

20III-S4-TVG1-1-2	Py	EPR1-2ºS	-0.62	0.04	-0.87	0.06	3								
20III-S4-TVG1-1-3	Py	EPR1-2ºS	-0.46	0.08	-0.68	0.13	3								
20III-S4-TVG1-1-4	Py	EPR1-2ºS	-0.58	0.11	-0.90	0.12	3								
20III-S4-TVG1-2-3	Py	EPR1-2ºS	-0.01	0.05	-0.08	0.11	3								
20III-S4-TVG1-2-3*	Py	EPR1-2ºS	-1.74	0.01	-2.58	0.09	3								
20III-S6-TVG3	Py	EPR1-2ºS	-1.20	0.01	-1.80	0.07	2								
20III-S4-TVG1-2-3	Cpy	EPR1-2ºS	0.11	0.09	0.19	0.03	3	-0.16	0.02	3					
IR05-TVG12-11	Py	EHF, CIR	-0.14	0.05	-0.18	0.08	3								
IR05-TVG12-14	Py	EHF, CIR	0.11	0.06	0.12	0.09	3								
19III-S18-TVG9	Py	EHF, CIR	-0.96	0.05	-1.43	0.06	6								
IR05-TVG13-4-1	Cpy	EHF, CIR	0.01	0.09	0.00	0.10	3	-0.57	0.09	3					
19III-S18-TVG9	Cpy	EHF, CIR	0.05	0.11	0.07	0.16	3	-0.88	0.13	3					
IR05-TVG12-5-2	Sp	EHF, CIR	-0.65	0.02	-0.93	0.08	3				-0.35	0.03	-0.17	0.02	3
IR05-TVG12-8-2	Sp	EHF, CIR	-0.85	0.08	-1.27	0.15	4				-0.47	0.03	-0.25	0.01	3
IR05-TVG12-8-4	Sp	EHF, CIR	-0.65	0.07	-0.93	0.09	3				-0.61	0.09	-0.30	0.06	3
IR05-TVG12-8-4*	Sp	EHF, CIR	-0.99	0.08	-1.45	0.20	3				-0.77	0.03	-0.39	0.02	3
IR05-TVG12-9-1	Sp	EHF, CIR	-1.65	0.07	-2.48	0.13	4				-0.43	0.00	-0.22	0.00	3
IR05-TVG12-11	Sp	EHF, CIR	-0.63	0.08	-0.98	0.15	3				-0.49	0.07	-0.26	0.02	3
IR05-TVG13-9.2-1	Sp	EHF, CIR	-1.34	0.02	-1.97	0.06	3				-0.45	0.11	-0.24	0.05	3
19II-S7-TVG4	Py	A area,	-1.96	0.04	-2.89	0.07	6								
21VII-TVG22	Py	A area,	-0.98	0.12	-1.47	0.06	4								
Back-arc basin sulfides (BABS)															
113.1GTV-1	Py	NFB	-0.98	0.15	-1.44	0.08	6								
113.1GTV-4	Py	NFB	-0.48	0.05	-0.73	0.06	3								
113.2GTV	Py	NFB	-1.20	0.07	-1.81	0.04	3								
113.1GTV-4	Cpy	NFB	-0.18	0.05	-0.25	0.10	3	-0.29	0.11	3					
26.1GTV-1	Sp	NFB	-0.99	0.02	-1.46	0.10	3				-0.44	0.05	-0.22	0.03	3
26.1GTV-2	Sp	NFB	-1.03	0.01	-1.50	0.10	3				-0.55	0.05	-0.28	0.03	3
26.2GTV-1	Sp	NFB	-0.90	0.02	-1.34	0.04	3				-0.03	0.07	-0.03	0.01	3
26.2GTV-3	Sp	NFB	-1.17	0.09	-1.77	0.17	3				-0.51	0.04	-0.25	0.03	3
Reference materials															
IRMM-014			0.00	0.03	0.01	0.08	25								
MIX			-1.55	0.12	-2.25	0.17	32								
Average Quality control 'Mix' on Nu Plasma I			-1.53	0.07	-2.26	0.15	6								
JMC Cu110 in-house								1.06	0.16	30					
SRM NIST 976 Cu								-0.97	0.13	27					
BHVO-2								0.00	0.07	9					
JMC Zn310 in-house											-0.20	0.09	-0.10	0.03	11
IRMM 3702 Zn											0.59	0.04	0.28	0.01	3
Lyon JMC 3-0749L Zn											0.00	0.03	0.00	0.04	3

* Indicates the analysis result of a duplicate sample.

Research Highlights

- Isotopically light Fe and heavy Zn fractionate into the fluid in fluid-basalt interactions.
- Plate subduction results in the enrichment of heavier Fe and lighter Zn isotopes in BAB and IA rocks.
- The Fe in the seafloor hydrothermal sulfides is mainly derived from the fluid.
- The ^{56}Fe, ^{57}Fe, and ^{63}Cu in the fluid are partitioned into the high-temperature sulfides.
- The fluids provide a source of heavy Cu and Zn isotopes to the plumes, seawater, and sediments.

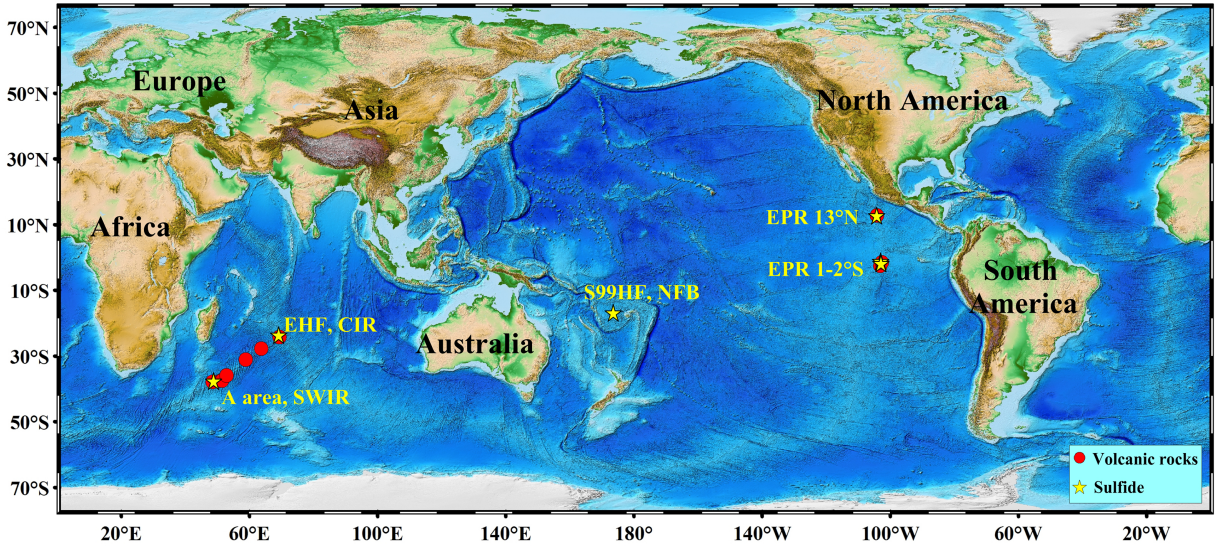
70°N
50°N
30°N
10°N
10°S
30°S
50°S
70°S
20°E
60°E
100°E
140°E
180°
140°W
100°W
60°W
20°W
Europe
Asia
Africa
North America
South America
Australia
EPR 13°N
EPR 1-2°S
S99HF, NFB
EHF, CIR
A area, SWIR
Volcanic rocks
Sulfide

Figure 1

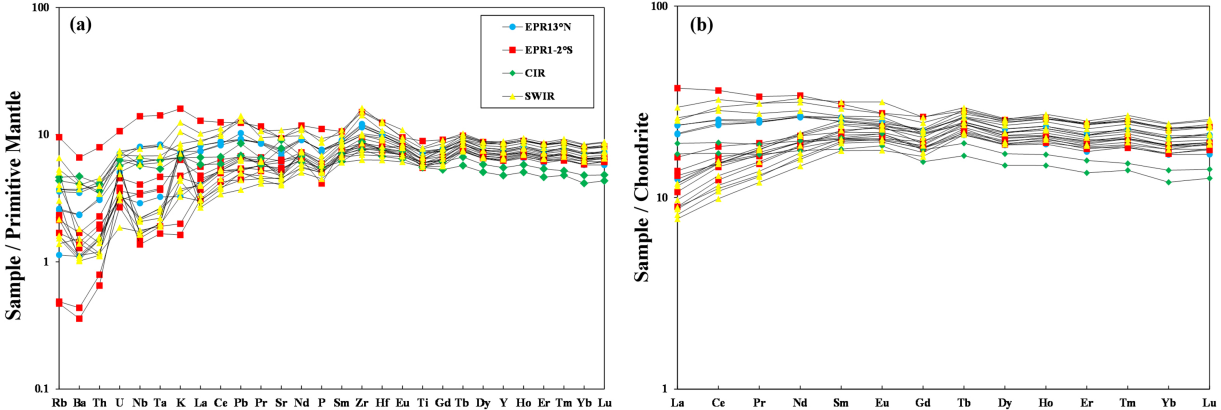
(a)
EPR13°N
EPR1-2°S
CIR
SWIR
Sample / Primitive Mantle
100
10
1
0.1
Rb Ba Th U Nb Ta K La Ce Pb Pr Sr Nd P Sm Zr Hf Eu Ti Gd Tb Dy Y Ho Er Tm Yb Lu
(b)
Sample / Chondrite
100
10
1
La Ce Pr Nd Sm Eu Gd Tb Dy Ho Er Tm Yb Lu

Figure 2

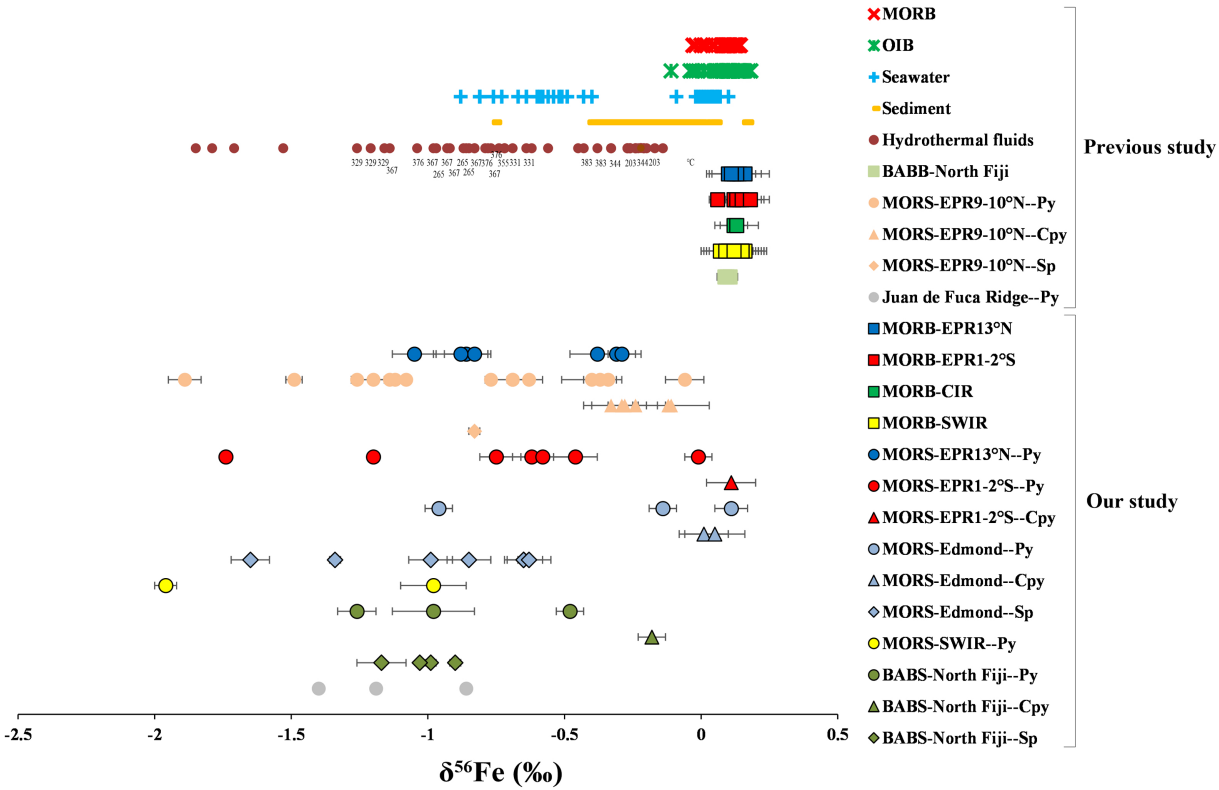
MORB
OIB
Seawater
Sediment
Hydrothermal fluids
BABB-North Fiji
MORS-EPR9-10°N--Py
MORS-EPR9-10°N--Cpy
MORS-EPR9-10°N--Sp
Juan de Fuca Ridge--Py
Previous study
MORB-EPR13°N
MORB-EPR1-2°S
MORB-CIR
MORB-SWIR
MORS-EPR13°N--Py
MORS-EPR1-2°S--Py
MORS-EPR1-2°S--Cpy
MORS-Edmond--Py
MORS-Edmond--Cpy
MORS-Edmond--Sp
MORS-SWIR--Py
BABS-North Fiji--Py
BABS-North Fiji--Cpy
BABS-North Fiji--Sp
Our study
-2.5
-2
-1.5
-1
-0.5
0
0.5
δ56Fe (‰)

Figure 3

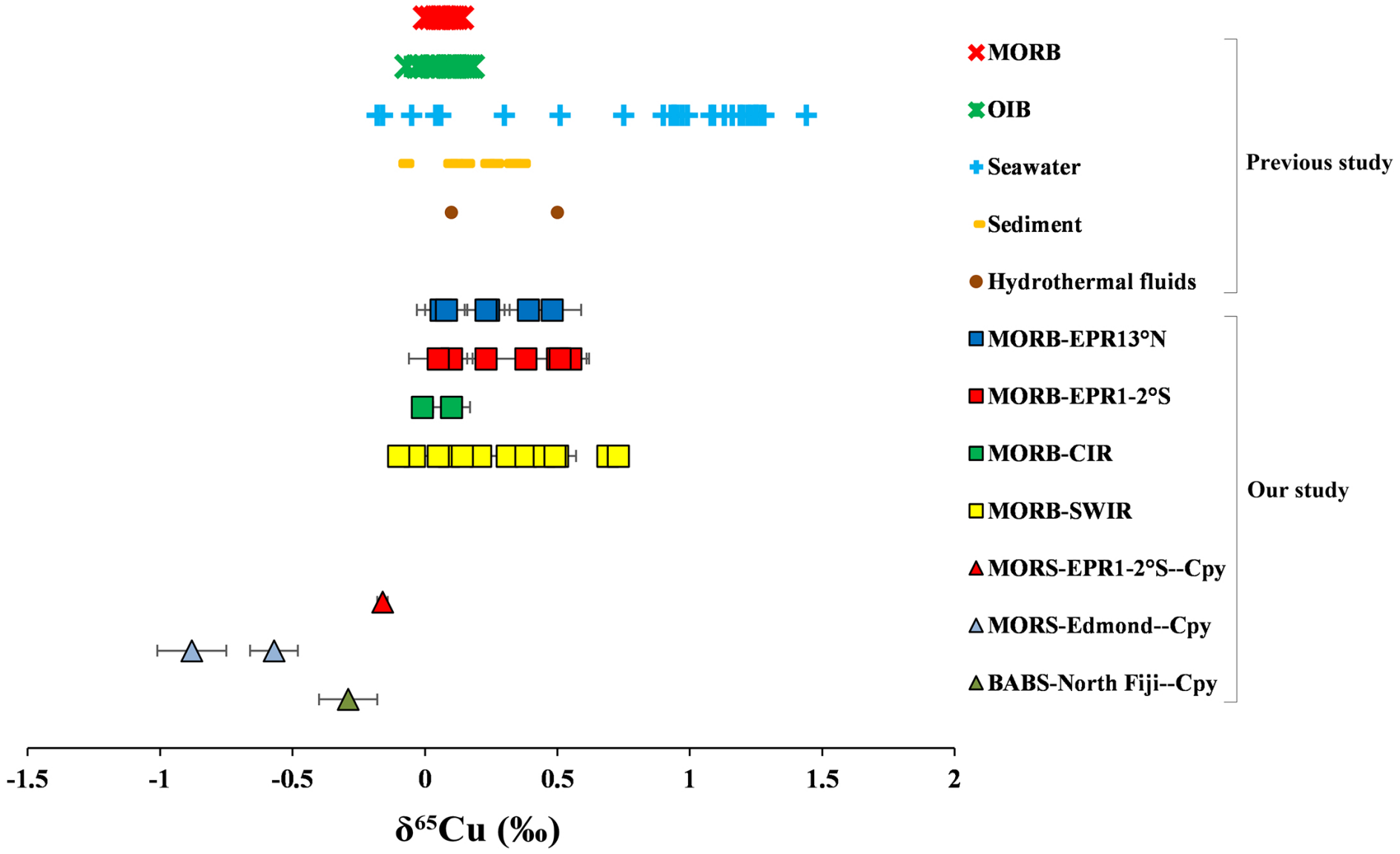
MORB
OIB
Seawater
Sediment
Hydrothermal fluids
Previous study
MORB-EPR13°N
MORB-EPR1-2°S
MORB-CIR
MORB-SWIR
MORS-EPR1-2°S--Cpy
MORS-Edmond--Cpy
BABS-North Fiji--Cpy
Our study
-1.5
-1
-0.5
0
0.5
1
1.5
2
δ65Cu (‰)

Figure 4

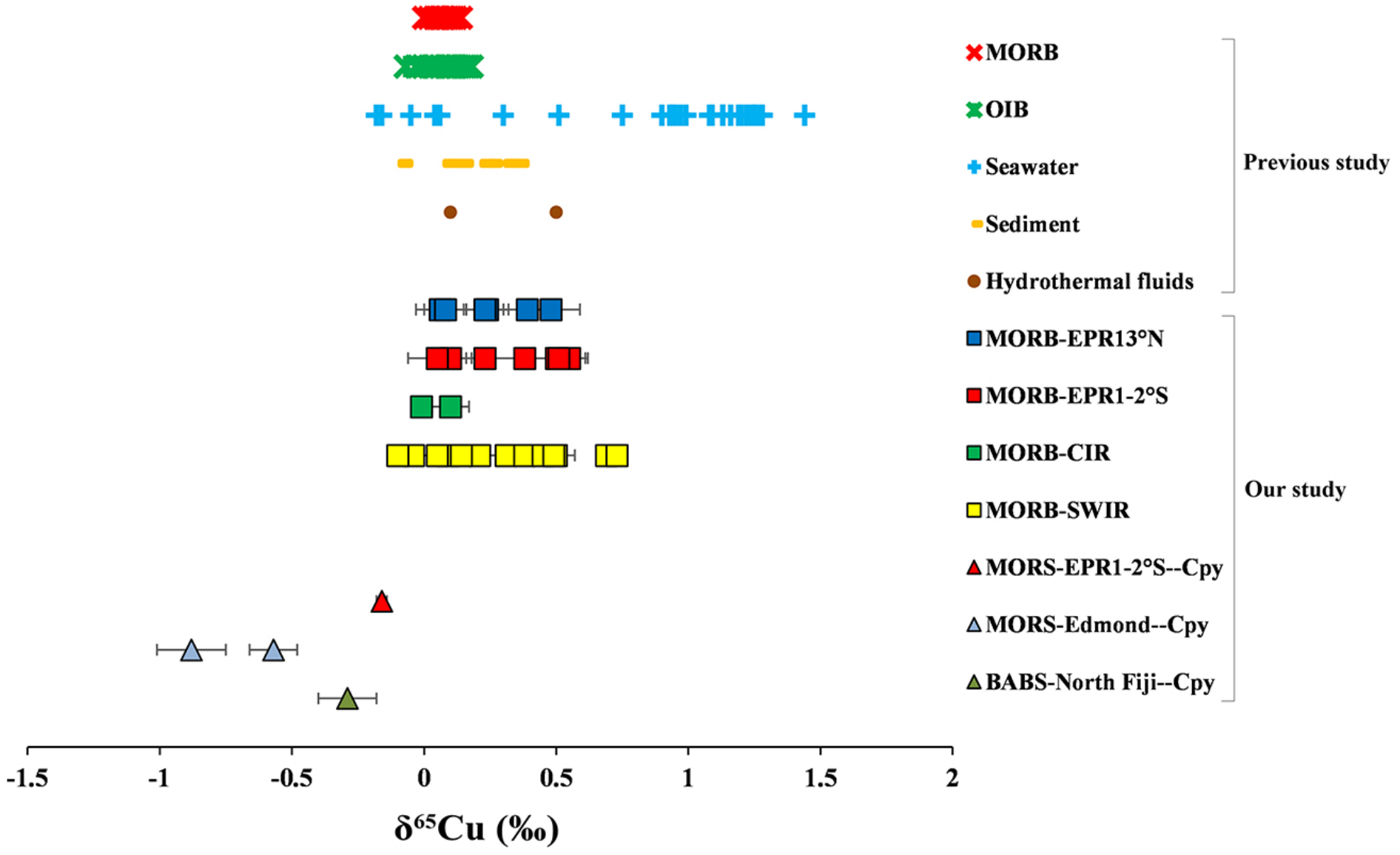
MORB
OIB
Seawater
Sediment
Hydrothermal fluids
Previous study
MORB-EPR13°N
MORB-EPR1-2°S
MORB-CIR
MORB-SWIR
MORS-EPR1-2°S--Cpy
MORS-Edmond--Cpy
BABS-North Fiji--Cpy
Our study
-1.5
-1
-0.5
0
0.5
1
1.5
2
δ65Cu (‰)

Figure 5

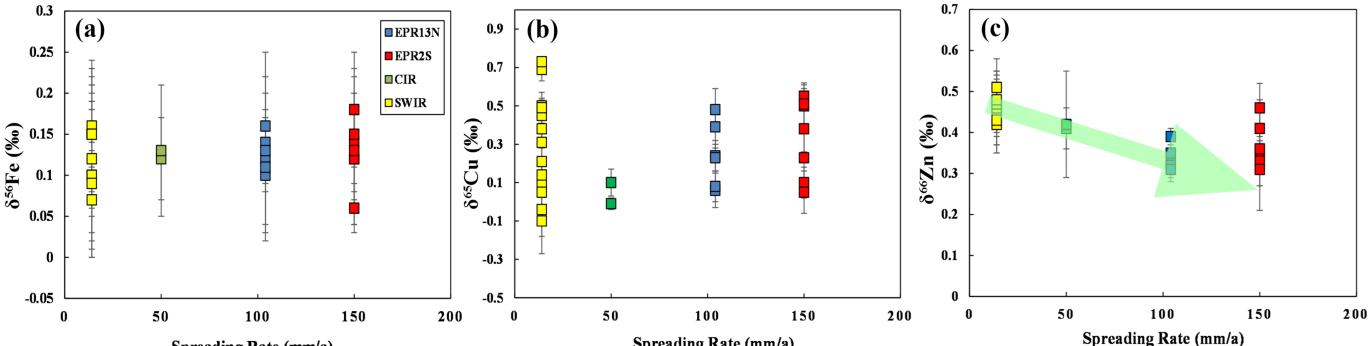
(a)
EPR13N
EPR2S
CIR
SWIR
δ56Fe (‰)
Spreading Rate (mm/a)
(b)
δ65Cu (‰)
Spreading Rate (mm/a)
(c)
δ66Zn (‰)
Spreading Rate (mm/a)

Figure 6

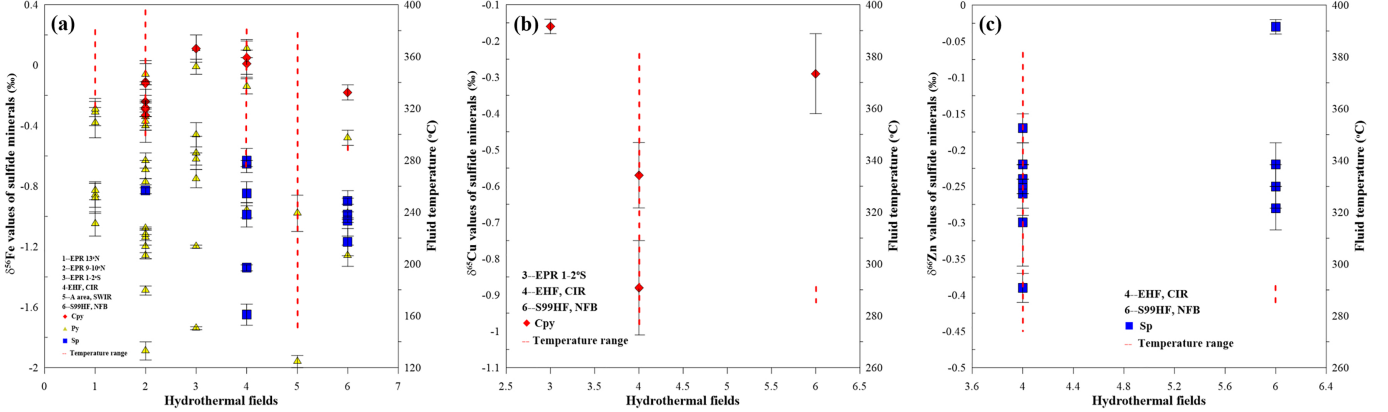
(a)
δ⁵⁶Fe values of sulfide minerals (‰)
Fluid temperature (°C)
Hydrothermal fields
1–EPR 13°N
2–EPR 9-10°N
3–EPR 1-2°S
4–EHF, CIR
5–A area, SWIR
6–S99HF, NFB
Cpy
Py
Sp
Temperature range
(b)
δ⁶⁵Cu values of sulfide minerals (‰)
Fluid temperature (°C)
Hydrothermal fields
3–EPR 1-2°S
4–EHF, CIR
6–S99HF, NFB
Cpy
Temperature range
(c)
δ⁶⁶Zn values of sulfide minerals (‰)
Fluid temperature (°C)
Hydrothermal fields
4–EHF, CIR
6–S99HF, NFB
Sp
Temperature range

Figure 7